Mon. Not. R. Astron. Soc. **000**, 1–?? () Printed 20 March 2013 (MN LATEX style file v2.2)

The planetary nebula Abell 48 and its [WN4] nucleus

David J. Frew[1,2⋆], I.S. Bojičić[1,2,3], Q.A. Parker[1,2,3], M. Stupar[1,2,3], S. Wachter[4], A. Danehkar[1,2], K. DePew[1,2], M.T. Fitzgerald[1,2] and D. Douchin[1,2]
[1]*Department of Physics and Astronomy, Macquarie University, Sydney, NSW 2109, Australia*
[2]*Research Centre in Astronomy, Astrophysics & Astrophotonics, Macquarie University, Sydney, NSW 2109, Australia*
[3]*Australian Astronomical Observatory, PO Box 296, Epping, NSW 1710, Australia*
[4]*Spitzer Science Center, California Institute of Technology, MS 220-6, Pasadena, CA 91125, USA*

Accepted ; Received ; in original form

ABSTRACT
We have conducted a detailed multi-wavelength study of the peculiar planetary nebula Abell 48 and its central star. We present evidence for a new classification of the nucleus as a helium-rich, hydrogen-deficient star of type [WN4], one of only two currently known examples of its type. The evidence for either a massive WN or a low-mass [WN] interpretation is critically examined, and we firmly conclude that Abell 48 is a planetary nebula (PN) around an evolved low-mass star, rather than a Population I ejecta nebula. Importantly, the surrounding nebula has a morphology typical of PNe, and is not enriched in nitrogen, and thus not the 'peeled atmosphere' of a massive star. We estimate a distance of 1.6 kpc and a reddening, $E(B-V)$ = 1.90 mag, the latter value clearly showing the nebula lies on the near side of the Galactic bar, and therefore cannot be a massive WN star. The ionized mass ($\sim$0.3 $M_{\odot}$) and electron density (700 cm^{-3}) are typical of middle-aged PNe. The observed stellar spectrum was compared to a grid of models from the Potsdam Wolf-Rayet (PoWR) grid. The best fit temperature is 71 kK, and the atmospheric composition is dominated by helium ($>$ 86 per cent by mass), with about 3–4 per cent nitrogen present. An upper limit on the hydrogen abundance is 10 per cent. Our results are in good agreement with the recent study of Todt et al. The unusually large nitrogen fraction is higher than any other low-mass H-deficient star, and is not explained by current post-AGB models. We give a discussion of the implications of this discovery for the late-stage evolution of intermediate-mass stars. There is now tentative evidence for two distinct helium-dominated post-AGB lineages, separate to the He+C dominated surface compositions produced by a late thermal pulse. Further theoretical work is needed to explain these recent discoveries.

Key words: planetary nebulae: general – planetary nebulae: individual: Abell 48 – stars: Wolf-Rayet – stars: evolution

1 INTRODUCTION

Classical Wolf-Rayet (WR) stars are massive hydrogen-deficient objects with powerful, fast winds and high mass-loss rates up to 10^{-4} M$_{\odot}$ yr^{-1} (Crowther 2007). Their spectra are characterised by strong, broad emission lines of helium, nitrogen, carbon or oxygen. A very similar phenomenon is found in some ionizing stars of planetary nebulae (PNe), which descend from less massive stars and are unrelated in an evolutionarily sense. These PN central stars (CSPN) are denoted as [WR] stars, utilising the square brackets introduced by van der Hucht et al. (1985) to avoid confusion with their massive analogues. While massive WR stars are predominantly nitrogen or carbon enriched (WN or WC types respectively), with a few higher temperature WO stars, almost all CSPNe catalogued to date belong to the [WC] and [WO] sequences (Tylenda et al. 1993; Crowther, De Marco & Barlow 1998; Acker & Neiner 2003).

In the course of a spectroscopic survey of detectable CSPNe (DePew et al. 2011), we were struck by the unusual nature of the central star of Abell 48 (PN G029.0+00.4), discovered and catalogued as a PN by Abell (1955, 1966). Abell 48 is a reddened, low-surface brightness object with a morphology resembling a thick torus or cylinder, possibly viewed nearly pole-on. Abell (1966) classified it as a double-ring nebula and gave an optical diameter of 40″. We used the SuperCOSMOS Hα Survey (Parker et al. 2005) to measure dimensions of 44″ $\times$ 39″. It has not been well studied optically due to its relative faintness.[1]

⋆ E-mail:david.frew@mq.edu.au

[1] Curiously, Helfand et al. (2006) classified it as a SNR candidate.

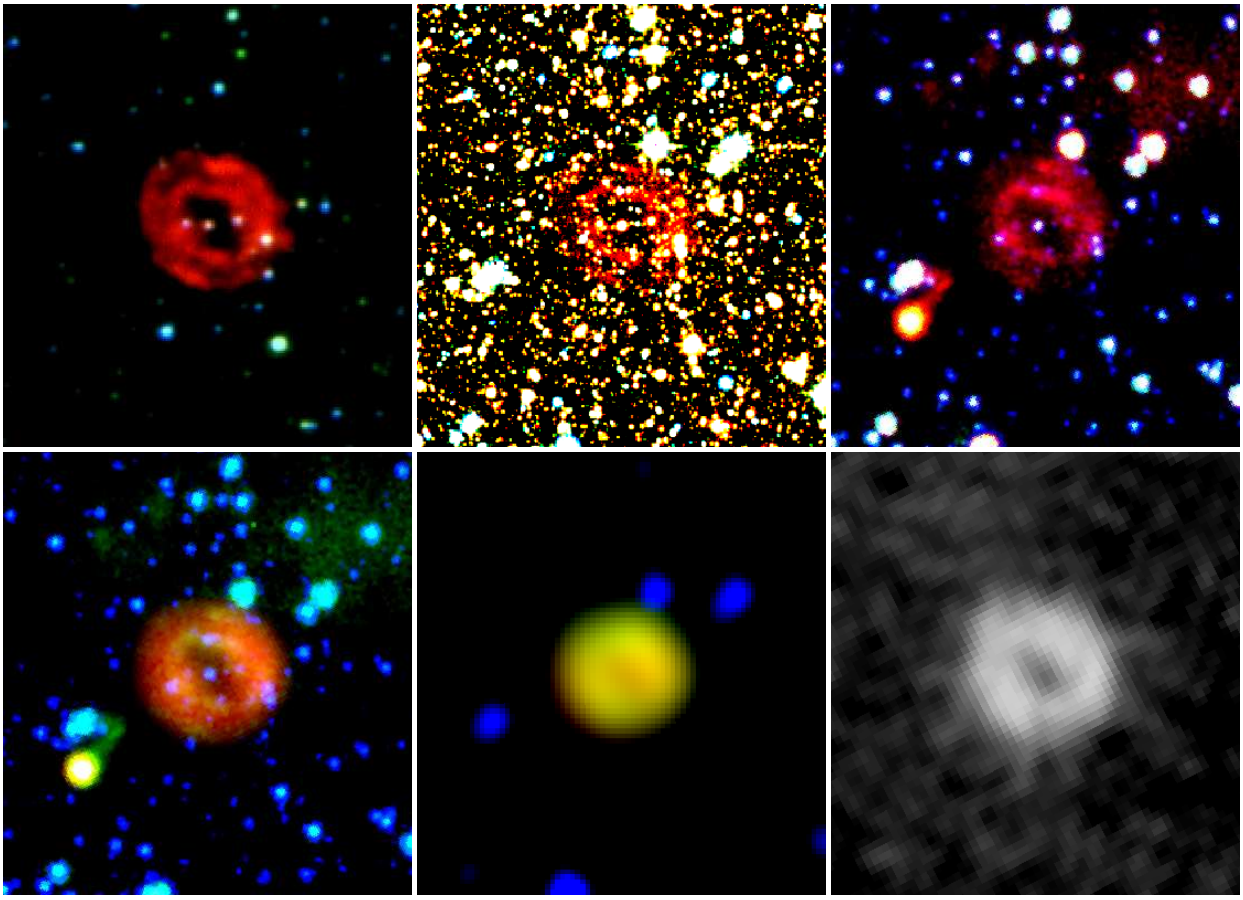

Figure 1. Montage of images for Abell 48, all to the same scale and orientation ($2.5' \times 2'$ with NE at top left), and with the colour palette set so that RGB channels map longer to shorter wavelengths respectively. Top row: At left is a composite B_J/R/Hα colour image of Abell 48. Note the elliptical, double-ring structure and the CSPN situated near the centre; Middle: UKIDSS JHK_s composite image; Right: GLIMPSE 3.6/4.5/8.0μm composite image. Bottom: Left: IRAC/MIPS composite 4.5/8.0/24μm image. Middle: WISE composite 3.4/11.6/22.1μm image; right: MAGPIS greyscale 20 cm radio image.

DePew et al. (2011) already concluded Abell 48 was a planetary nebula and gave a preliminary classification of the CSPN as [WN] or [WN/C], but since the important CIV λ5806 doublet was *unobserved* in that work, a more precise spectral type could not be ascertained at time. Independently, Wachter et al. (2010) classified the central source as a Population I WN6 star, in contrast to the system's previous long association as a PN (Abell 1966; Perek & Kohoutek 1967; Acker et al. 1992; Kohoutek 2001). This uncertainty led us to more closely investigate this interesting object and tie down its identification.

In this paper we present a detailed multi-wavelength study of Abell 48 and its central star, expanding on the preliminary analysis reported in Bojičić et al. (2012). As this paper was completed, an independent study of this object was published by Todt et al. (2013, hereafter TK13), coming to essentially the same conclusions as us. We will refer to their results in the context of our own paper where necessary. We have confirmed Abell 48's CSPN as a hydrogen-poor [WN] star, as first suggested by DePew et al. (2011). We also explore the nature and characteristics of the proposed [WN] and [WN/WC] CSPNe, based on a comparison of Abell 48 to the other candidate [WN] and [WN/C] stars, their possible progenitors, and their likely progeny (Todt et al. 2010a,b, 2012; TK13; Werner 2012; Miszalski et al. 2012b, hereafter MC12).

This paper is arranged as follows: we describe our new observations of Abell 48 in § 2, undertake a detailed analysis of the nebula and its central star in § 3 and § 4, discuss the evidence for its nature as a PN in § 5. In § 6 we review the [WN] or [WN/C] classes, discuss the possible evolutionary pathways of these groups in § 7, before giving our conclusions and suggestions for future work in § 8.

2 OBSERVATIONS

2.1 Spectroscopic Observations

Optical spectra of Abell 48 and its central star were obtained on the ANU 2.3-metre telescope at Siding Spring Observatory using the Wide Field Spectrograph (WiFeS; Dopita et al. 2007, 2010), on 1 July 2009. WiFeS has a double-beam configuration, with spectral resolutions of 3000 or 7000m, and a $38'' \times 25''$ field of view with a spatial resolution of $1''$. Since the angular size of Abell 48 is larger than this, the instrument was positioned on the northern section of the nebula (including the CSPN) to make sure that some suitable background sky was available for subtraction. This was an early run during WiFeS commissioning time so the more effective nod-and-shuffle mode was not used. Low resolution gratings (B3000 and R3000) were employed and the exposure time on target was 1500s. Thin cloud was present during the observation.

Table 1. Spectroscopic and photometric observations of Abell 48 utilised in this study.

Date	Telescope	Instrument	λ Range	$R = \Delta\lambda/\lambda$	Exp. time
2008 Sep 4	Hale 200-in	Dual Spectrograph	3400–5600, 5850–8300	1000	900
2009 Jul 1	ANU 2.3m	WiFeS	3400–5900, 5300–9600	2900	1500
2010 Apr 22	ANU 2.3m	WiFeS	4180–5580, 5300–7060	6900	1200
2012 Aug 23	ANU 2.3m	WiFeS	3400–5900, 5300–9600	2900	1200
Date	Telescope	Instrument	Filter	...	Exp. time
2012 Feb 24	2.0m FTN	Merope Camera	B	...	900
2012 Mar 14	2.0m FTN	Merope Camera	I_c	...	10
2012 May 8	2.0m FTN	Merope Camera	BV	...	200, 150
2012 May 18	ANU 2.3m	Imager	$UBVI_c$	...	300, 2×300, 2×180, 2×120

Higher resolution gratings (B7000 and R7000) were used on a second run in April 2010. This observation was aimed at getting kinematic data on the nebula, so the IFU was positioned to cover both the CSPN and centre of the nebula. A further exposure of the southern section of the nebula was taken using WiFeS at low resolution in August 2012. The night was photometric and consequently the S/N ratio is best on this spectrum. For the WiFeS data, the frames were bias subtracted and flux- and wavelength-calibrated using the WiFeS data reduction pipeline in conjunction with standard IRAF routines (see Dopita et al. 2010). The flux calibration was performed using the spectrophotometric standard star LTT 3864.

We also utilised the spectrum of the central star first presented by Wachter et al. (2010), obtained with the 5.0-m Hale telescope at Palomar Observatory on 4 September 2008 using the Double Spectrograph. This spectrograph also has a two-arm configuration, utilising a dichroic to split the light in to two channels, observed simultaneously. The 316 line mm^{-1} grating in first order, dichroic D55 and a slit width of 1″ were used. The resulting spectra cover 4000–5600 Å and 5800–8300 Å with a dispersion of 2.0 and 2.4 Å pixel^{-1} on the blue and red sides, respectively, with a spectral resolution of 5–7 Å. FeAr (blue) and HeNeAr (red) arcs were used for wavelength calibration. Bias and flat-field corrections to the raw spectrum images were performed using standard IRAF routines. A log of the observations is presented in Table 1.

2.2 Photometric Observations

New optical photometry of the central star was also obtained with the Australian National University's 2.3-m reflector at Siding Spring Observatory (SSO) in May 2012, and the 2.0-m Faulkes Telescope North (FTN) at Haleakala Observatory, Maui, in queue mode on three different nights in 2012. A log of the observations is presented in Table 1. For the SSO run, the standard imager at the f/18 Nasmyth focus was used. This used Bessell $UBVI_c$ filters were in front of a 2048×2048 pixel thinned E2V CCD. The pixel size is 13.5μm, giving a plate scale of 0.34″/pixel across a 6.6′ circular field of view. The seeing was modest ($\sim$1.5″) and the night was photometric. Standard extinction coefficients were applied, and a range of standard stars from Landolt (2009) were measured to determine the colour equations used to convert from instrumental magnitudes.

For the FTN observations (see Table 1), the Merope camera at the f/10 focus was used with BVI_C Johnson-Cousins filters. The camera utilised an E2V CCD with 2048 2048 pixels, in 2 ×2 binning mode, giving images 4.7′ on a side with a plate scale of 0.28″/pixel. The averaged observed magnitudes are presented in § 4.1.

2.3 Archival Data

To supplement our spectroscopic and photometric data, we made an extensive search for archival multi-wavelength data of the nebula and central star using the Aladin Sky Atlas[2], and the SkyView Virtual Observatory[3]. Narrowband Hα (+ [N II]) images were obtained from the SuperCOSMOS Hα Survey (SHS; Parker et al. 2005; Frew et al. 2013c) and the Southern H-Alpha Sky Survey Atlas (SHASSA) (Gaustad et al. 2001). Broadband images of the nebula and star were also obtained from the SSS (Hambly et al. 2001), 2MASS (Skrutskie et al. 2006), and UKIDSS (Lawrence et al. 2007) surveys in the optical and near-IR, and the GLIMPSE (Benjamin et al. 2003; Churchwell et al. 2009), MIPSGAL (Carey et al. 2009), and WISE (Wright et al. 2010) mid-IR surveys.

Continuum fluxes for the nebula (and the central star separately if available), were retrieved from the VizieR service or measured from the original images as part of this work. We also downloaded 20 cm and 90 cm high-resolution MAGPIS images (Helfand et al. 2006) to supplement the NVSS radio data (Condon & Kaplan 1998). Figure 1 shows a multiwavelength montage of merged-colour images for Abell 48, all to the same scale. We adopt the best position for the central star from the 2MASS catalogue. The fundamental observable properties of the nebula are summarised in Table 2.

3 THE PLANETARY NEBULA

3.1 Nebular Morphology

Abell 48 has an apparent 'double-ring' morphology with a lozenge-shaped interior cavity (see Figure 1), which might be the projection of a thick torus or cylinder viewed nearly pole-on, as has been kinematically demonstrated for other morphologically similar nebulae (e.g. O'Dell et al. 2013). There is also a pair of point symmetric knots or enhancements which are prominent in the [N II] λ6584 line (see Figure 2), and which are often seen in PNe. This fact, the PN-like morphology seen in Hα images, and the emission measure of the ionized nebula all indicate that it is material recently ejected by the central star, and not simply windswept interstellar material (see the morphological atlas of WR shells by Gruendl et al. 2000). This fact has important implications for the origin of the nebula, as we elucidate below.

Soker (1997), on the basis of its morphology, hinted that the central star of Abell 48 may be a binary system (see later). If this

[2] Accessible from the Centre de Donnés Astronomiques de Strasbourg (CDS).
[3] http://skyview.gsfc.nasa.gov/

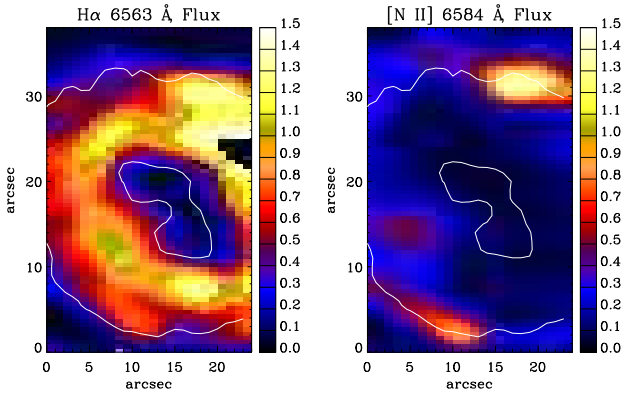

Figure 2. Surface brightness maps of Abell 48 in the Hα and [N II]λ6584 lines, extracted from the WiFeS observation of Apr 2010. Note the pair of opposing knots which are prominent in the [N II] λ6584 line. Flux units are in 10^{-15} erg cm^{-2}s^{-1} per spaxel.

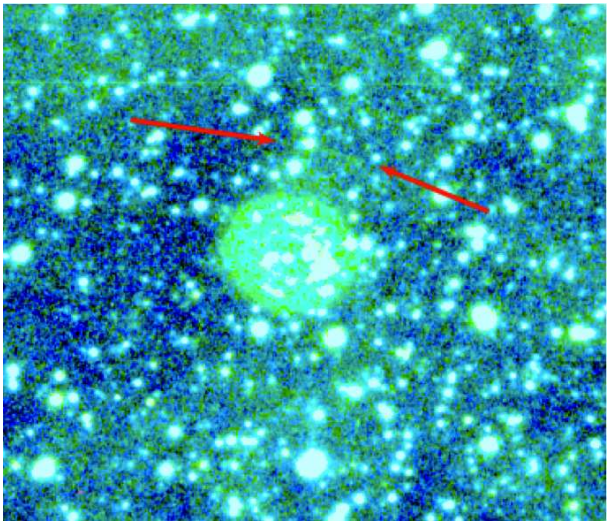

Figure 3. A deep continuum-subtracted (Hα / broadband R) SHS image of Abell 48 showing two short arcs, the outer one arrowed, located 40$''$ and 45$''$ north-west of the CSPN.

turns out to be true, a binary evolution channel may be implicated to explain the unusual surface abundances of the central star, as has been suggested for the LMC PN, N 66 (Hamann et al. 2003) and for the peculiar, N-enhanced central star of the Eskimo nebula, NGC 2392 (e.g. Méndez et al. 2012). The nebular emission-line profiles (see section 3.3.3, below) also appear to rule out simple spherical symmetry (cf. López et al. 2012), so we tentatively interpret the double shell morphology as due to the geometric orientation of two opposing lobes. A full morpho-kinematic analysis of the nebula, based on our WiFeS imaging data, will be the subject of a future paper (Danehkar et al., in prep.), but a preliminary analysis indicates this is the likely scenario at play.

To the northwest of the PN there appear to be two faint closely spaced arcs about 30$''$ in extent, with the outermost being 45$''$ from the CSPN (see Figure 3). These arc-like structures were first noted by DePew (2011) and there also appears to be evidence of a very faint, discontinuous, elliptical halo on deep continuum-subtracted SHS Hα images, discovered as part of the survey of Frew, Bojičić & Parker (2012)[4]. The overall dimensions are about 280$''$ $\times$ 210$''$ in extent, but deep CCD images are needed to confirm them. Together, these features may provide evidence for earlier AGB mass-loss events.

Even though Abell 48 is very close to the Galactic mid-plane, where the density of the interstellar medium (ISM) is highest (Spitzer 1978), the PN has no observable signature of an ISM interaction (Borkowski, Sarazin & Soker 1990; Soker, Borkowski & Sarazin 1991; Pierce et al. 2004; Wareing et al. 2006; Wareing 2010; Frew et al. 2011; Ali et al. 2012). Therefore the peculiar velocity of the CSPN is likely to be low (<40 km/s). However, TK13 claim Abell 48 is a runaway star, based on the CSPN's proper motion of 19.5 mas yr$^(-1)$ in p.a. 222° from the PPMXL catalogue (Roeser, Demleitner & Schilbach 2010). However the proper motion from the USNO-B1.0 catalogue (Monet et al. 2003), 25.3 mas yr$^(-1)$ in p.a. 342°, differs from this value. Owing to the faintness of the central star, these catalogue values may be spurious.

[4] The SHS is an excellent search medium for faint structures surrounding PNe and related objects (see also Miszalski et al. 2012a).

Table 2. Observed parameters of Abell 48.

Property	Value	Reference
RA (J2000)	18 42 46.92	2MASS
Dec (J2000)	$-$03 13 17.3	2MASS
Size	44$''$ $\times$ 39$''$	This work
F(Hα)	2.7 ($\pm$ 0.2) $\times$ 10^{-12} erg cm^{-2}s^{-1}	This work
$F_{\lambda5007}$	0.5 ($\pm$ 0.2) $\times$ 10^{-12} erg cm^{-2}s^{-1}	This work
$E(B-V)$	1.90 $\pm$ 0.2	This work

3.2 Integrated Nebular Fluxes

We have four independent estimates of the integrated Hα flux for Abell 48. Frew et al. (2013a) derived log$F$(Hα) = $-$11.52 $\pm$ 0.09 (in cgs units) from flux-calibrated SHASSA data (Gaustad et al. 2001), while Frew et al. (2013b) estimated log$F$(Hα) = $-$11.56 $\pm$ 0.15 from newly-calibrated SuperCOSMOS Hα images (Parker et al. 2005), in good agreement. We also used our WiFeS IFU data, scaling up the integrated Hα fluxes to account for the portion of the nebula that was not observed. We did this for two separate runs to obtain log$F$(Hα) = $-$11.59 and $-$11.62 respectively. The weighted mean flux of all estimates is log F(Hα) = $-$11.58 $\pm$ 0.06 erg cm^{-2}s^{-1}, and this value was adopted in conjunction with our newly measured 1.4 GHz radio flux of 200 mJy to derive an independent reddening value (see § 3.3.1).

A full summary of all continuum flux measurements of the nebula is given in Table 3. In the radio-continuum domain we found two catalogued but highly discrepant values for the 1.4 GHz (20 cm) integrated flux density of Abell 48; $S_{1.4}$ = 159 $\pm$ 15 mJy from the NRAO VLA Sky Survey (NVSS; Condon et al. 1998; Condon & Kaplan 1998) and $S_{1.4} \approx$ 657 mJy, catalogued in the Multi-Array Galactic Plane Imaging Survey (MAGPIS; Helfand et al. 2006). The discrepancy is too large to be attributed to confusion by the complex background, as noted by Condon & Kaplan (1998). Therefore, we re-measured the flux density from the MAGPIS and NVSS total intensity images[5] using the KARMA data analysis pack-

[5] The images were downloaded from the NVSS and MAGPIS postage

Table 3. Summary of continuum flux measurements for Abell 48.

Wavelength (μm)	Flux (mJy)	Survey	Reference
3.6	67 ± 7	IRAC	C11
4.5	109 ± 10	IRAC	C11
5.8	32 ± 5	IRAC	C11
8.0	244 ± 24	IRAC	C11
8.3	375 ± 15	MSX	EP03
11.6	1195 ± 120:	WISE	FB13
14.7	2053 ± 125	MSX	EP03
18	3341 ± 42	AKARI	I10
21.3	1735 ± 110	MSX	EP03
22.1	1600 ± 200	WISE	FB13
24	2065 ± 100	MIPSGAL	M10, PM11
25	2530 ± 250	IRAS	IPAC
60	<2070	IRAS	IPAC
65	29020 ± 570^a	AKARI	I10
70	11000 ± 2000	MIPSGAL	FB13
90	30990 ± 2200^a	AKARI	I10
140	48930 ± 15100^a	AKARI	I10
160	59040 ± 11700^a	AKARI	I10
6 cm	>70	MAGPIS	FB13
6 cm	<400	NVSS	FB13
11 cm	$\geqslant 220$	VLA	PB03,FB13
20 cm	159 ± 15	NVSS	CK98
20 cm	200 ± 20	MAGPIS	FB13
90 cm	60 ± 10	MAGPIS	FB13
$[F_{12}/F_8]$	0.69	...	FB13
$[F_{24}/F_8]$	0.93	...	FB13
$[F_{70}/F_{12}]$	1.07	...	FB13
$[F_{70}/F_{24}]$	0.82	...	FB13

Flux sources: C11 – Cohen et al. (2011); CK98 – Condon et al. (1998); EP03 – Egan et al. (2003); FB13 – this work; I10 – Ishihara et al. (2010); IPAC – IPAC (1986); M10 – Mizuno et al. (2009); PB03 – Paladini et al. (2003); PM11 – Phillips & Marquez-Lugo (2011); ^{a} Fluxes are confused with surrounding emission.

age (Gooch 1996). While our estimated flux density from the NVSS image agrees with the catalogued value within the uncertainties, we measured a flux of ≈200 mJy from the MAGPIS image, significantly at odds with the catalogued value, but closer to the NVSS flux. In fact the published MAGPIS fluxes need to be revised (D. Helfand, 2011, private communication), so the catalogued value of 657 mJy is erroneous.

However, the superior resolution of the MAGPIS image allows us to filter out the large structures close to Abell 48 and avoid the confusion problem which affects the NVSS data, so we adopt our new MAGPIS measurement for further analysis. In addition, we measured the flux density at 0.325 GHz (90 cm) from an intensity image taken as a part of the MAGPIS survey (for more details see Helfand et al. 2006). Both flux values are tabulated in Table 3, along with several additional integrated flux measurements of the nebula taken from the literature. It is clearly seen from these fluxes that the emission from the nebula is thermal in nature, typical of photoionized gas.

stamp servers – NVSS: http://www.cv.nrao.edu/nvss/ and MAGPIS: http://third.ucllnl.org/gps/

3.2.1 Infrared Fluxes

The nebula is faint in 2MASS and UKIDSS images. In the K_s band, which has the strongest detection, we attribute the flux to molecular hydrogen (H_2) at 2.122μm, as well as the Brγ 2.166μm hydrogen line (Kimeswenger et al. 1998). The GLIMPSE data resolves the nebula well, and it appears brightest in the IRAC2 and IRAC4 bands. On this basis, the Brα 4.05 μm line is probably the strongest feature contributing to the IRAC2 flux, and strong polycyclic aromatic hydrocarbon (PAH) bands (Allamandola, Tielens & Barker 1989) are the likely main contributor to the IRAC4 flux, particularly the bands at 7.7 and 8.6 μm, with some emission from Pfα 7.46μm and the Ar III 8.99μm fine-structure line. We ran a preliminary photoionization model to test these predictions using the three-dimensional photoionization code `MOCASSIN` (Ercolano et al. 2003, 2005). The photoionization model predicts a flux for the Ar III 8.99μm line of around 20% of Hβ. A full description and analysis will be published separately (Danehkar et al, in prep.).

The WISE 432 and 321 false-colour composites appear greenish-yellow and red respectively, reflecting the relative strength of the WISE3 band at 12 microns. Features that may contribute to this band are PAH emission, particularly at 11.3 μm, thermally-emitting dust continuum, and the [S IV] 10.51μm line which our photoionization model suggests is comparable in strength to Hβ. Other features contributing to this band, in order of decreasing strength are the [Ar III] 8.99μm, [Ne III] 15.5μm, and [Ne II] 12.8μm lines. Indeed, MIR false-colour imaging has proven to be a powerful diagnostic indicator for classification purposes in their own right (e.g. Cohen et al. 2007, 2011; Parker et al. 2012).

Abell 48 is a moderately strong source in the MIPS 24μm band (Mizuno et al. 2009; Wachter et al. 2010),[6] considering that the [O IV] fine-structure line is expected to be weak or absent on the basis of the nebular excitation class. Our optical spectrum (see Figure 5) shows the nebula to be of relatively modest excitation (§ 3.3), with no detectable emission lines with an ionization potential (I.P.) exceeding 41.0 eV, based on the weak detection of the [Ne III] λ3869 line in the violet. This suggests that warm dust is the main contributor to the 24μm band, with a minor contribution from the [Ar III] 21.81μm line.

The spectral energy distribution (SED) of the nebula, not shown here, is dominated by this warm dust component. From a blackbody fit to the thermal IR fluxes given in Table 3 we estimate a dust temperature of 150 K, which is much more typical of PNe, rather than the hotter dust which surrounds massive WR stars (van der Hucht et al. 1985). Mizuno et al. (2009) also found that the 8μm emission in the shell was co-spatial with the 24μm emission. Similarly, we find that the NIR and MIR dimensions are similar to the optical and radio images indicating that the ionized, molecular, and dust components of the nebula are spatially mixed.

3.3 Nebular Spectroscopy

Our three different WiFeS data cubes were used to investigate the nebular conditions. Figure 4 presents individual slices of the low-resolution (R = 3000) and medium-resolution (R = 7000) WiFeS red-arm spectra respectively. The broad features from the CSPN, the respective nebular and night sky line strengths, and line-splitting of the nebular lines due to expansion can be seen. The 1-D low-resolution spectrum from 2012, binned from the data cube to

[6] Mizuno et al. (2009) list this source as MGE 029.0781+00.4547.

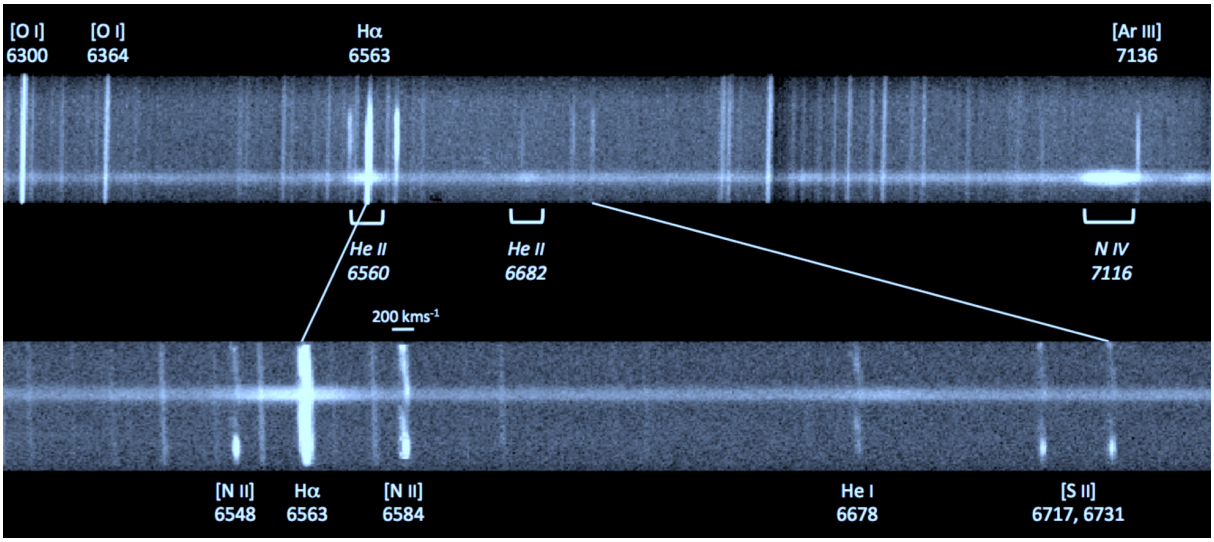

Figure 4. Individual image slices of our low-resolution (R = 3000; top panel) and medium-resolution (R = 7000; bottom panel) WiFeS red spectra showing the broad features from the CSPN, and line-splitting of the nebular lines due to expansion.

increase the signal to noise (S/N) ratio, is illustrated in Figure 5. It shows the presence of a bright nebular Hα line and relatively weak [N II] $\lambda\lambda$ 6548,84 lines in the red, a steep Balmer decrement due to the relatively high extinction, as well as fairly weak [O III] lines in the blue relative to Hβ. There is no indication of a nebular He II λ4686 line (to a level of 1% percent of Hβ).

In Table 4, we summarise the observed and reddening-corrected line fluxes. The other WiFeS spectra were used to confirm that the faintest nebular lines were real. The nebular spectrum presented by TK13 is similar to our own, the main difference being that TK13 estimated a somewhat higher extinction. However, owing to the rather low decimal excitation class, EC = 1.45 (Dopita & Meatheringham 1990; Reid & Parker 2010), we conclude that the weak λ7236 feature that we also detected is more likely to be a C II recombination line rather than the forbidden [Ar IV] line on the basis of our photoionization model.

3.3.1 *Reddening*

A summary of the various reddening determinations is presented in Table 5. We have derived the logarithmic extinction at Hβ using the Balmer decrement of the nebular lines in our three independent WiFeS spectra, where the intrinsic line strengths from Hummer & Storey (1987) and the reddening law of Howarth (1983) have been used. We also determine $c_{\rm H\beta}$ = 2.6 by comparing the 1.4 GHz radio flux with our integrated Hα flux in the usual way (e.g. Bojičić et al. 2011b), and an independent, albeit lower accuracy reddening estimate using the equivalent width of the λ6284 diffuse interstellar band (DIB) and applying the relation of Friedman et al. (2011). We also utilised the Pζ/Hα decrement, again adopting the line strengths from Hummer & Storey (1987). The value of A_V = 5.7 mag quoted in Wachter et al. (2010) for this object translates to an extinction coefficient of $c_{\rm H\beta}$ = 2.7. We re-evaluated this parameter by fitting the overall SED of the star, excluding the IRAC [8.0]-mag value, which is uncertain, to determine $E(B-V)$ = 1.90 $\pm$ 0.10, or $c_{\rm H\beta}$ = 2.75 (see § 4.4).

We adopt an averaged reddening, $E(B-V)$ = 1.90 $\pm$ 0.10 ($c_{\rm H\beta}$ = 2.75) hereafter. This value can also be compared with the estimate of $E(B-V)$ = 2.1 ($c_{\rm H\beta}$ = 3.0) from DePew et al. (2011), based on the nebular Balmer decrement from a shallow MSSSO 2.3-m spectrum, while TK13 determined $E(B-V)$ = 2.10 from a SED fit, and $E(B-V)$ = 2.15 from the Balmer decrement method.

3.3.2 *Plasma Diagnostics*

We estimated the nebular density of Abell 48 to be n_e = 700 cm^{-3} from the observed ratio of the [S II] doublet. The [N II] λ5755 line is barely detected giving an uncertain value of the electron temperature, while the far red [S III] lines were used to estimate $T_{\rm e}$ = 7000 K, and another low quality estimate comes from the ratio of the auroral to nebular [O II] lines. Two further estimates come from the relative strengths of the He I lines (Zhang et al. 2005). Despite the larger uncertainties of some of the fainter diagnostic lines, the independent estimates of the electron temperature are in good agreement, and we adopt an average value of 7500 K for the abundance analysis (§ 3.4). A summary of the plasma diagnostics is presented in Table 6.

3.3.3 *Expansion Velocity*

There do not appear to be any expansion velocity measurements for Abell 48 in the literature, so we used the WiFeS red-arm medium-resolution spectrum, taken in April 2010, to estimate the expansion velocity of the nebula from the width of the brightest nebular emission lines. The observed FWHM for each line was determined using the *splot* function in IRAF, and the expansion velocity, corrected for instrumental resolution and thermal broadening, was calculated with the following expression:

$$v_{\rm exp} = 0.5\,({\rm FWHM}^2_{\rm obs} - {\rm FWHM}^2_{\rm instr} - 8(\ln 2) k\,T_{\rm e}/m)^{0.5} \quad (1)$$

where k is Boltzmann's Constant, $T_{\rm e}$ is the electron temperature taken from section 3.3 and m is the atomic mass of the ion. The HWHM is often taken to be equal to the expansion velocity, but we instead use V_{10} (Medina et al. 2006) which is a better proxy for the expansion of the outer nebular rim (e.g. Schönberner et al. 2005).

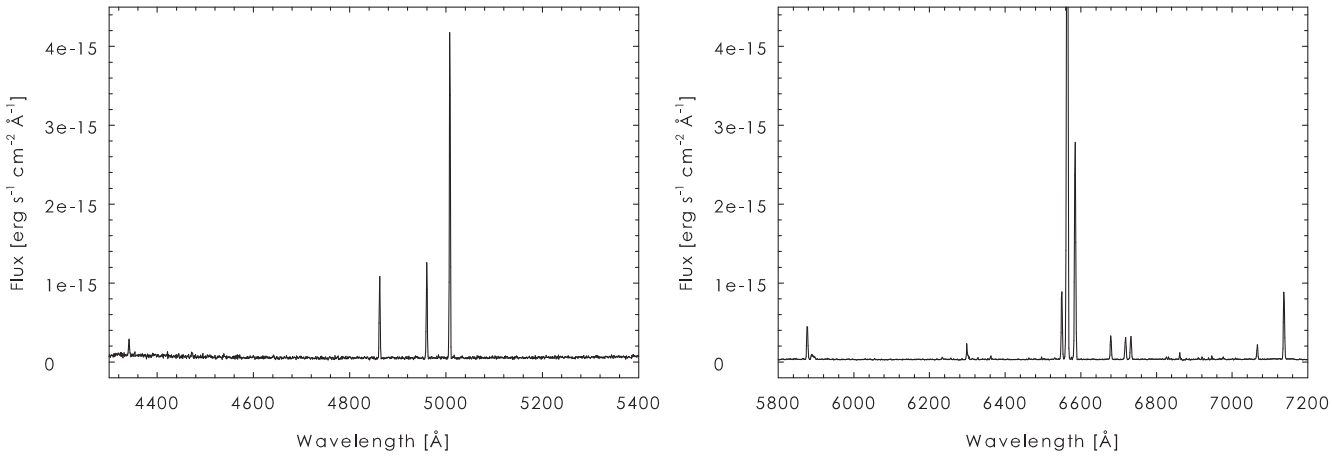

Figure 5. Extracts of the integrated blue (left) and red spectra of Abell 48, obtained from the high S/N WiFeS observation from 2012.

Table 4. List of emission line fluxes for Abell 48, adopted from the high S/N WiFeS IFU spectrum from 2012; 'n.m.' means the line was detected but not measured.

Line	λ	$f(\lambda)$	$F(\lambda)$	$I(\lambda)$
[O II]	3727	0.256	13:	64:
[Ne III]	3869	0.230	6.8:	28:
Hδ	4101	0.182	n.m.	n.m.
Hγ	4340	0.127	19.9:	43.5:
[O III]	4363	0.121	<1.0	<2.1
He I	4471	0.095	5.0:	9.0:
He II	4686	0.043	<0.8	<1.0
Hβ	4861	0.000	100	100
[O III]	4959	-0.024	119	103
[O III]	5007	-0.036	402	322
He I	5016	-0.038	n.m.	n.m.
[N II]	5755	-0.195	1.3:	0.40:
He I	5876	-0.215	67.6	17.9
[S III]	6312	-0.283	2.1:	0.37:
[N II]	6548	-0.318	138	19.4
Hα	6563	-0.320	2056	286
[N II]	6583	-0.323	429	58.4
He I	6678	-0.336	43.7	5.5
[S II]	6716	-0.342	42.3	5.1
[S II]	6731	-0.344	44.1	5.3
He I	7065	-0.387	28.0	2.6
[Ar III]	7136	-0.396	129	11.2
C II	7231	-0.408	n.m.	n.m.
C II	7236	-0.409	12.9:	1.0:
He I	7281	-0.414	12.1	0.94
[O II]	7320	-0.419	10.3:	0.78:
[O II]	7330	-0.420	7.2:	0.54:
[Ar III]	7751	-0.467	33.8	1.9
[Cl IV]	8046	-0.497	n.m.	n.m.
P16	8502	-0.540	25:	0.9:
P15	8545	-0.542	16:	0.6:
P14	8599	-0.547	13:	0.4:
P13	8665	-0.553	29:	0.9:
P12	8750	-0.560	29:	0.9:
P11	8863	-0.569	35:	1.0:
P10	9015	-0.581	20:	0.6:
[S III]	9069	-0.585	787	21.3
Pζ	9229	-0.597	94.6	2.4

Table 5. A summary of the various reddening determinations for Abell 48 which are all in good agreement.

Method	$E(B-V)$
SED	1.90 ± 0.10
Radio/Hα flux	1.77 ± 0.15
Hα/Hβ decrement[1]	2.2 ± 0.2
Hα/Hβ decrement[2]	1.92 ± 0.1
Hα/Hβ decrement[3]	1.85 ± 0.1
Pζ/Hα decrement[1]	2.2 ± 0.2
Pζ/Hα decrement[3]	1.8 ± 0.2
λ6284 DIB	1.9 ± 0.5
Adopted reddening	1.90 ± 0.15
Asymptotic reddening[†]	10.0 ± 2.0

[1]From WiFeS spectrum 1; [2]WiFeS spectrum 2; [3]WiFeS spectrum 3; [†]Schlafly & Finkbeiner (2011)

Table 6. Summary of plasma diagnostics for Abell 48

Diagnostic	Value	Result
[S II] λ6717/λ6731	0.96	$N_{\rm e}$ = 700 cm^{-3}
[N II] (λ6548+λ6584)/λ5755	195:	$T_{\rm e}$ = 7600 K:
[O II] λ3727/(λ7320+λ7330)	77:	$T_{\rm e}$ = 6700 K:
[S III] (λ9069+λ9532)/λ6312	198	$T_{\rm e}$ = 6700 K:
[O III] (λ4959+λ5007)/λ4363	>210:	$T_{\rm e} < 9950$ K
He I λ7281/λ5876	0.17	$T_{\rm e}$ = 7300 K
He I λ7281/λ6678	0.053	$T_{\rm e}$ = 7700 K
Gas temperature (adopted)	...	$T_{\rm e}$ = 7500 K

We derive V_{10} = 40 kms^{-1}, which agrees with the average expansion velocity of sample of [WC] PNe, $v_{\rm exp}$ of 36 km s^{-1} (Peña et al. 2003). From the same data-set we measure a heliocentric radial velocity of +36 $\pm$ 3 kms^{-1}, obtained using the IRAF package `emsao`, which is lower than the velocity of +50 $\pm$ 4 kms^{-1} determined by TK13. Our measurement translates to a velocity relative to the local standard of rest of $v_{\rm LSR}$ = +49 $\pm$ 3 kms^{-1}.

This observed expansion velocity also falls in the range seen for LBV and WNL shells (Nota et al. 1995; Chu 2003), but we point out that no coherent, point-symmetric, moderate-density ejecta shell is known to surround any massive WNE star. The earliest spectral type seen in a high-surface brightness coherent nebula is

Table 7. Ionic abundances, adopted ionization correction factors and total abundances for Abell 48.

Line, λ(Å)	Ion	Abundance
5876, 6678	He^{+}/H^{+}	0.129
	ICF(He)	1.00
	He/H	0.129
6548, 6584	N^{+}/H^{+}	2.21(−5)
	ICF(N)	2.75
	N/H	6.07(−5)
3727, 7325	O^{+2}/H^{+}	1.76(−4)
4957, 5007	O^{+2}/H^{+}	3.13(−4)
	ICF(O)	1.00
	O/H	4.89(−4)
3869	Ne^{+2}/H^{+}	1.10(−4)
	ICF(Ne)	1.57
	Ne/H	1.73(−4)
6717, 6731	S^{+}/H^{+}	5.51(−7)
6312, 9069	S^{+2}/H^{+}	1.15(−5)
	ICF(S)	1.10
	S/H	1.33(−5)
7136	Ar^{+2}/H^{+}	2.10(−6)
	ICF(Ar)	1.57
	Ar/H	3.30(−6)

Table 8. Summary of photometric measurements for the [WN4] central star of Abell 48. The third column gives the dereddened magnitudes.

Waveband	m	m_0	Source
U	19.8 ± 0.2	10.6	FB13
B	19.48 ± 0.02	11.7	FB13
V	17.80 ± 0.01	11.9	FB13
V	17.72 ± 0.25	11.8	YB6
I	15.50 ± 0.05	12.0	DENIS
I_c	15.14 ± 0.05	11.7	This work
J	13.54 ± 0.09	11.8	DENIS
J	13.508 ± 0.027	11.7	2MASS
J	13.440 ± 0.002	11.7	UKIDSS
H	12.834 ± 0.028	11.7	2MASS
H	12.823 ± 0.001	11.7	UKIDSS
K_s	12.302 ± 0.11	11.6	DENIS
K_s	12.325 ± 0.027	11.6	2MASS
K_s	12.281 ± 0.002	11.6	UKIDSS
[3.6]	11.69 ± 0.06	11.3	GLIMPSE
[4.5]	11.25 ± 0.10	11.0	GLIMPSE
[5.8]	11.06 ± 0.09	10.8	GLIMPSE
[8.0]	11.04 ± 0.16	10.8	GLIMPSE

References for photometry: FB13 (this work); YB6 (Zacharias et al. 1994); DENIS (Epchtein et al. 1994); 2MASS (Skrutskie et al. 2006); UKIDSS (Lawrence et al. 2007); GLIMPSE (Benjamin et al. 2003).

WN7b for PMR 5 (Frew et al., in prep). Earlier WN stars possess increasingly one-sided shells, fragmented by Rayleigh-Taylor instabilities and having abundances diluted in part by swept-up gas from the diffuse ISM. An example is NGC 6888 (Gruendl et al. 2000; Fernández-Martn et al. 2012) around the WN6b(h) star WR 136.

3.4 Nebular Abundances

We derived ionic and total nebular abundances from our spectra using the EQUIB code (see Wesson, Stock & Scicluna 2012), after adopting the values of T_e and N_e given in Table 6. We determined the helium abundance from the measured intensities of the λ5876 and λ6678 He I recombination lines using the effective recombination coefficients from Hummer & Storey (1987). For the metallic ions, the abundances were derived from the observed line intensities of the strong collisionally-excited lines. We then derived the total abundances using the ionization correction factors (ICFs) derived from the expressions given in Kingsburgh & Barlow (1994). Note that the oxygen abundance is somewhat uncertain, as the nebular λ3727 [O II] doublet has an uncertain flux due to the high extinction in the blue. Furthermore, the neon abundance is only an indicative estimate, owing to the similarly poor S/N ratio of the λ3869 [Ne III] line. The abundances and adopted ICFs are presented in Table 7.

Our analysis shows that Abell 48 has no significant enrichment of nitrogen (N/O $\approx$ 0.12) and does not belong to Peimbert's Type I class (Peimbert 1978; Peimbert & Torres-Peimbert 1983), for which we adopt Kingsburgh & Barlow's (1994) definition of N/O $>$ 0.8. In fact, the nebular abundances are approximately solar, a point to which we return below. Here we differ from the conclusions of TK13, who find slightly subsolar abundances for Abell 48. We attribute this discrepancy to the higher electron temperature they adopt. We do not detect the [O III] λ4363 line which sets an upper limit on the electron temperature of $\sim$10 kK, and the mean of several independent diagnostics suggests a lower temperature of 7500 K (see Table 6), and hence a higher derived oxygen abundance. We will revisit the nebular abundances in § 5.2, § 6 and § 7.2.

4 THE CENTRAL STAR

4.1 Photometry

The central star is obvious on SuperCOSMOS B_J, R_F, I_N, and Hα images (Hambly et al. 2001; Parker et al. 2005), as well as 2MASS, UKIDSS and GLIMPSE images (Skrutskie et al. 2006; Lawrence et al. 2007; Benjamin et al. 2003). We summarise the available literature photometry of the central star in Table 8, along with the $UBVI$ magnitudes derived from our optical photometry. In order to correct the observed magnitudes and colours for reddening, a colour excess of E$(B-V)$ = 1.90 mag is adopted from section 3.3.1. The visual absorption is then A_v = 5.9 mag using the reddening law of Howarth (1983).

No time series photometry of the central star is available, so information on any short-period variability is lacking. However J and K_s magnitudes are available from three different epoch surveys, DENIS, 2MASS and UKIDSS (Epchtein et al. 1994; Skrutskie et al. 2006; Lawrence et al. 2007) and all agree within the uncertainties, so we can tentatively say the star is not a large amplitude variable, unlike the ionizing star of the LMC planetary N 66 (SMP 83) (McKibben Nail & Shapley 1955), which is likely to host an interacting binary system (Hamann et al. 2003).

4.2 Spectroscopy

Spectroscopic classifications of the central star of Abell 48 were undertaken by Wachter et al. (2010) and DePew et al. (2011). Wachter et al. (2010) classified the central star as a WN6 according to the classification scheme developed by Conti, Massey & Vreux (1990). The previous shallow MSSSO 2.3m spectrum presented in DePew et al. (2011) showed a broad feature at λ7116Å in the red, but a large section of the spectrum between 5050Å and 6300Å was

Table 9. Principal emission lines found in the CSPN of Abell 48.

Species	λ (Å)	$-W_\lambda^1$ (Å)	$-W_\lambda^2$ (Å)	FWHM (km s^{-1})
He II	3203	...	n.m.	...
N IV	3480	...	45:	1300:
N IV	3748	...	3.0:	...
N IV	4058	...	23:	830
He II+N III	4100	...	29:	1060
He II+N III	4200	...	15:	800
He II	4339	...	11.5	800
N III	4379	...	6.0:	...
N III	4518	...	12:	...
He II	4542	n.m.	16:	1200
N V	4604	n.m.	22.5	560
N V	4620	n.m.	19.5	600
N III	4634-40	...	12:	...
He II	4686	...	160	1170
He II	4860	...	21.5	1120
N III	4905	...	2.0:	...
N V	4944	3.0:	10:	...
N IV	5202	5.4	5.0:	...
He II	5411	23	34	900
C IV	5806	...	15.2	1300:
He I	5876	3.8	n.m.	...
He II	6118	4.0	2.2	
He II	6171	...	2.3	...
He II	6311	8.0	5.4	...
N IV	6382	3.8:	6.8:	800
He II	6406	7.1	7.9	...
He II	6527	4.3	6.6	...
He II	6560	130:	n.m.	1020
He I+He II	6683	...	...	blend
He II	6891	11.4	10.4	750
N IV	7116	160	130	1300
He II	7178	16.7	...	...
He II+N IV	7590	n.m.	9.8	450:
He II	8237	40.3	31.1	850
He II	8856	...	...	600
He II	9225	7.9	...	700

[1] WiFeS spectrum; [2] Hale spectrum

not observed, so it was unclear whether this was a [WN] or [WN/C] star.

In our deep WiFeS spectra, we again find a strong feature centred around λ7116Å, attributed to the complex of N IV lines between λ7103Å and λ7129Å. The He II λ6560 line appears as a broad (FWHM$\sim$25Å) feature from which the nebular Hα line protrudes (the nebular lines are over-subtracted in the Palomar data). The He II λ4686 and λ5412 lines are prominent and a broad C IV $\lambda\lambda$5801,12 doublet is also present, as is typical of the WN class.

We measured the stellar emission lines from all of our spectra using the `splot` function in IRAF. Based on the presence of the N IVλ4057, and N V$\lambda\lambda$4604,20 being much stronger than the N IIIλ4634,40 blend, with relatively weak C IV, we revisited the classification and now classify it as [WN4], primarily following the criteria given by Smith, Shara & Moffat (1996), giving most weight to the ratio of the equivalent widths of the He IIλ5411 and He Iλ5876 lines. We also made use of our low-resolution WiFeS stellar spectrum, which extends to $\sim$9500Å, but little in the way of classification schemes use the far red / near-IR wavelength region. As part of another project, we downloaded all the red spectra of the Galactic WN stars presented by Hamann, Koesterke & Wessolowski (1995), and measured the equivalent width of the λ8237 He II line for each star, if available. We tabulated the He II/He I ratios and spectral type from Smith et al. (1996) for each and found, as expected, a tight relation between the two quantities. This relation was then used to estimate a spectral class of [WN4] for the CSPN of Abell 48. Table 9 presents the identifications, the line equivalent widths (in Å), and the line widths (FWHM in kms^{-1}) of the principal lines that were clearly detected, while the numerical criteria we used to classify the star are summarised in Table 10. Our adopted classification is [WN4], while TK13 estimated a spectral class of [WN5].

Table 10. Classification of the central star, following the scheme of Smith et al. (1996). The second column is the ratio of the measured equivalent widths.

Criterion	Ratio	Classification
$W_{\lambda5411}/W_{\lambda5876}$	9.5	WN4
$W_{\lambda8237}/W_{\lambda5876}$	7.8	WN4
P_{5411}/P_{5876}	2.6	WN5
P_{4604}/P_{4640}	1.6	WN5
$P_{4057}/P_{4604-40}$	0.8	WN4
P_{5808}/P_{5876}	1.6	WN5
P_{5808}/P_{5411}	0.6	WN4-5
Adopted	...	[WN4]

We further note that there is no obvious indication of an oscillating Pickering decrement (e.g. Smith et al. 1996), showing that the star is hydrogen deficient. To quantitatively estimate the hydrogen fraction, we use the 'Pickering index' defined by Smith et al. (1996; cf. Oliveira, Steiner & Cieslinski 2003):

$$\frac{N(\mathrm{H}^+)}{N(\mathrm{He}^{++})} = \frac{W(\lambda4859+\lambda4861)}{[W(\lambda4541)\times W(\lambda5411)]^{0.5}} - 1 \qquad (2)$$

Formally, we obtain the unphysical value of -0.1, which we reset to zero. In practice, we adopt a working upper limit for the hydrogen abundance of $\sim$10% based on the observed S/N of the lines. Overall the spectrum is very similar to a Population I WN4o star (Vreux, Dennefeld & Andrillat 1983; Smith et al. 1996), but as we show in Section 5, the intrinsic properties of the surrounding nebula unambiguously show that we are dealing with low-mass PN central star.

4.3 Model Atmosphere Analysis

To begin the analysis, we downloaded the synthetic spectra appropriate for WNE model atmospheres from the Potsdam Wolf-Rayet (PoWR) database[7] (Hamann & Gräfener 2004) to compare with our data. These spectra are determined from the PoWR model atmospheres, described in Gräfener, Koesterke & Hamann (2002) and Hamann & Gräfener (2003), which account for spherical expansion, non-LTE effects, and metal line blanketing. The PoWR model grid has two dimensions, the stellar temperature T_* and the "transformed radius," R_t (Hamann & Koesterke 1998), which is a wind density parameter, being a function of the mass-loss rate, $\dot{M}$, and the stellar radius, R_*. It is given by:

$$R_\mathrm{t} = R_* \left[\frac{v_\infty}{2500\ \mathrm{km\,s^{-1}}} \Big/ \frac{\dot{M}\sqrt{D}}{10^{-4}\ M_\odot\ \mathrm{yr^{-1}}} \right]^{2/3} \qquad (3)$$

where v_∞ is the terminal velocity of the wind and D is a wind

[7] See http://www.astro.physik.uni-potsdam.de/$\sim$wrh/PoWR/powrgrid1.html

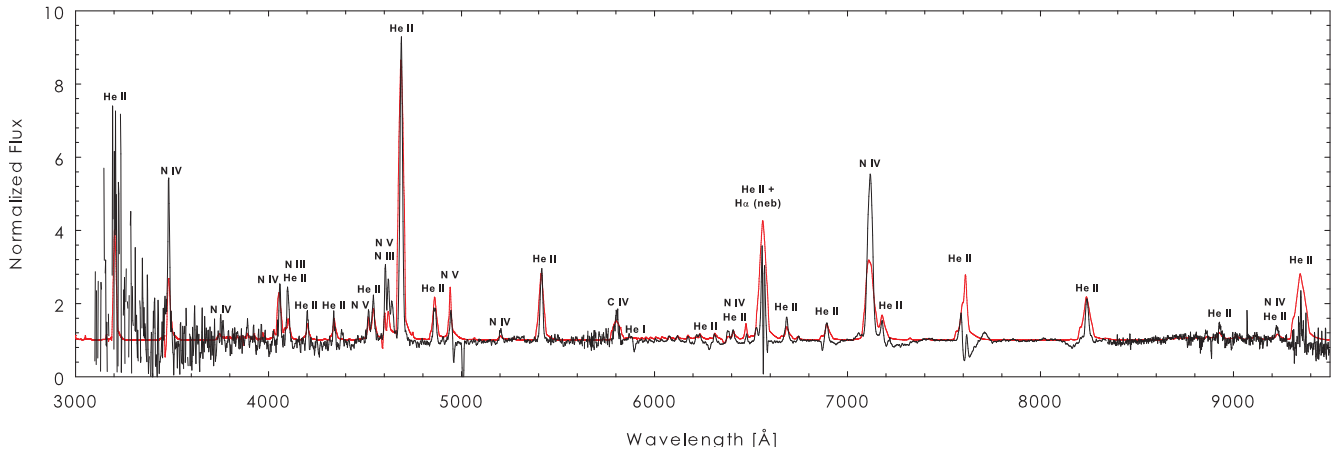

Figure 6. Normalized spectrum (black line) of the central star, spliced from our WiFeS and Palomar data. Note the presence of the N V $\lambda\lambda$4604,4620 lines and the very prominent He II λ4686 and N IV λ7116 features in the spectrum. Overplotted is an updated model 10-13 (red line) from the Potsdam Wolf-Rayet (PoWR) grid, (provided by H. Todt), which fits the relative strengths of the He lines well. The relatively poor fit to the nitrogen lines suggests the default nitrogen abundance is at least a factor of two too low, and should be instead around 3 – 4 per cent.

clumping factor (or inverse of the filling factor). It has been previously noted that many parameters of massive WRs and [WR]s are similar (e.g. Crowther, Morris & Smith 2006), a consequence of the scaling law for WR atmospheres first noted by Schmutz, Hamann & Wessolowski (1989). In other words, two atmospheres with the same temperature (T_*) and transformed radius ($R_{\rm t}$) show very similar spectra regardless of L_*, R_*, $\dot{M}$ and v_∞.

The PoWR grid models are normalized to $L/L_\odot$ = 2.0×10^5 which is appropriate for a massive WN star; consequently, the stellar flux of our CSPN is proportional to L_*, and R_* and $\dot{M}$ are proportional to $L_*^{1/2}$ and $L_*^{3/4}$ respectively. We follow Hamann & Koesterke (1998) in assuming a wind clumping factor of D = 4 (f = 0.25), which is appropriate for WN stars. The stellar radius, R_*, is the inner boundary of the model atmosphere and corresponds by definition to a Rosseland optical depth of 20. The stellar effective temperature, T_*, is the effective temperature at R_*, and can be easily calculated from the Stefan-Boltzmann law:

$$L = 4\pi R_*^2 \sigma T_*^4 \quad (4)$$

For Abell 48, various line ratios using the N III, N IV and N V, and He I and He II lines, initially constrained the temperature to between 63 and 79 kK and log ($R_t/R_\odot$) between 0.6 and 1.0. The absence of He IIλ4686 emission in the surrounding nebula is due to the optically thick WR wind. Models with $T_{\rm eff}$ < 60kK show a He I λ5876 line much stronger than observed, while models with $T_{\rm eff}$ > 90 kK are ruled out as these produce significant flux shortward of the HeII ionization edge at 228Å, so He II emission should be clearly present in the surrounding nebula. The estimated temperature is in broad agreement with the temperature range of 60–90 kK found for massive WN4 stars by Hamann & Gräfener (2003).

The best-fit model has $T_{\rm eff}$ = 71 kK and $R_{\rm t}$ = 6.3 $R_\odot$ (model 10-13) and reproduces fairly well the relative equivalent widths of the helium lines. A new synthetic spectrum calculated from a revised model 10-13, which utilised updated atomic data was kindly provided by H. Todt (2013, pers. comm.) The model parameters are $T_{\rm eff}$ = 71kK and logR_t = 0.8, with the default abundances set to He:C:N:O = 0.98: 1E-4: 0.015: 0.0. The synthetic spectrum is plotted along with our observed spectrum in Figure 4.2). However, the N III, N IV and N V line intensities are all weaker in the model, in particular the N V 4944 and N IV 7116 blends. This indicates that the default nitrogen abundance is too low, and that nitrogen is enhanced by a factor of at least ∼2 over the PoWR model. We have not convincingly detected any line due to oxygen, so we make no modification to the default model abundance. Our parameters are in excellent agreement with that derived by TK13 (see their Table 3).

The main difference between the two independent studies is that TK13 estimate a somewhat higher nitrogen abundance of 5 percent and a hydrogen abundance of 10 per cent, a result that does not disagree with our upper limit for this element. So it is now apparent that the photospheric nitrogen and hydrogen abundances differ considerably between Abell 48 and IC 4663, mimicking the range of H abundances seen in the O(He) stars (Reindl et al. 2012, and references therein).

The intrinsic luminosity of the star, and hence its distance, is not constrained from the model atmosphere analysis. Instead we adopt the distance of 1.6 kpc from § 5.3 in the discussion that follows, cf. TK13 who assumed a canonical post-AGB luminosity. We found the bolometric correction of the model atmosphere to be −5.4 mag, which leads to an estimated luminosity of the star of ∼5.5 ×10$^3 L_\odot$.

From our adopted value of the temperature T_*, the stellar radius R_* was calculated using equation 4 to be 0.49 $R_\odot$. From the line widths presented in Table 9, we estimate a terminal wind velocity, v_∞ of 1200 kms^{-1}. Finally, we estimate the mass-loss rate, $\dot{M}$, which is proportional to $L^{3/4}$ for a constant $R_{\rm t}$ (equation 3). We determine log $\dot{M}$ = -6.3 ± 0.2 $M_\odot$ yr^{-1}.

4.4 Stellar Spectral Energy Distribution

The stellar spectral energy distribution (SED) for the CSPN of Abell 48 is shown in Figure 7, along with the adopted PoWR model atmosphere. The model has been normalized to the ensemble of the dereddened values from Table 8, excluding the Johnson U band and IRAC 8.0 micron magnitudes, which are both uncertain. We applied the optical reddening law of Howarth (1983) and the IR extinction law of Indebetouw et al. (2005). The photometric points are fit very well by the model set at 71 kK, and a reddening c_β = 2.75.

There is no evidence from our spectra for any signature of a companion star, nor from the SED for any near-IR excess due

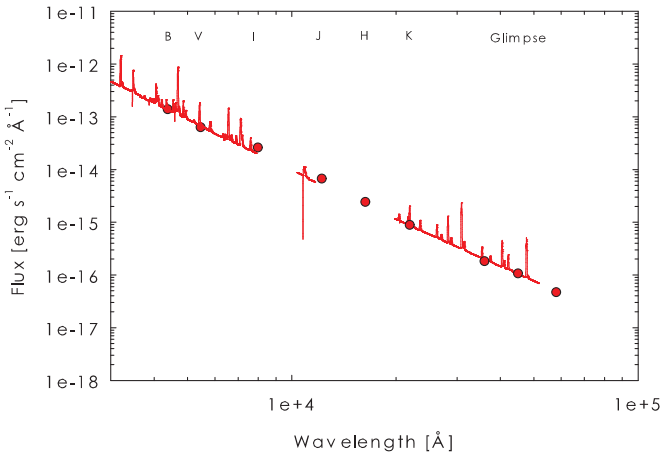

Figure 7. The spectral energy distribution of the central star of Abell 48. The red line shows the adopted model spectrum (PoWR model 10–13), with the photometric measurements dereddened with $E(B-V)$ = 1.90 plotted as red circles.

to a cooler companion (Douchin et al. 2012; De Marco et al. 2013), though in this case any limit is not strong. The [WN] star is relatively luminous and the near-IR magnitudes include a non-negligible contribution from wind free-free emission. As a result, any companion with a spectral-type later than ∼F0 V would not be detected. The tentative absence of variability (§4.1) suggests the star does not have an irradiated binary companion (De Marco, Hillwig & Smith 2008; Miszalski et al. 2009; Hajduk, Zilstra & Gesicki 2010), so time-series spectroscopic analysis is probably the best way to determine if Abell 48 is a binary (Jorissen & Frankowski 2008). However, at orbital periods greater than a year or two, the expected velocity shifts of the emission lines would be likely too small to be detected against the stochastic variations of the stellar wind.

5 DISCUSSION

As a precursor to any discussion on the evolutionary implications of the [WN] class, it is crucially important to try to properly compile and assess all the observational evidence pertaining to Abell 48 so that its status as a true PN or a circumstellar ring nebula around a massive star can be made clear. Circumstellar nebulae can be morphologically similar to PNe, and are found around several types of massive stars (Chu 2003; FP10; Mizuno et al. 2010; Wachter et al. 2010; Gvaramadze, Kniazev & Fabrika 2010; Bojičić et al. 2011a).

5.1 Diagnostic plots

Figure 8 shows the SMD (Sabbadin, Minello & Bianchini 1977) or log F(Hα)/F [NII] versus log F(Hα)/F [SII] diagnostic diagram (Sabbadin, Minello & Bianchini 1977) as extensively updated by Frew & Parker (2010, hereafter FP10), and further refined here.

Individual PNe are shown as small red dots and Galactic H II regions as small black squares. In the left panel the fields showing HII regions, SNRs and PNe are marked; note the considerable overlap between them. The blue triangles show the PNe with confirmed [WN] or [WN/C] stars, Abell 48, IC 4663, PB 8, along with NGC 6572, which has a candidate [WN/C] CSPN (Todt et al. 2012). These all plot squarely in the PN domain, while the orange diamond is N 66, the only PN in the LMC with a [WN] ionizing star. It shows substantial nitrogen enrichment compared to the mean LMC abundance.

In the right panel the domain of LBV/WR ejecta is plotted, and the green triangles plot a selection of ejecta nebulae. These are all nitrogen enriched from CNO cycling, and mostly overplot the Type I PN region defined by FP10. Clearly, Abell 48 falls in the PN domain away from both Type I PNe and and the CNO processed ejecta around LBV and WNL stars. This confirms our nebular abundance analysis (§3.4 and §5.2) showing the nebula is not strongly enriched in nitrogen, and therefore highly unlikely to be the product of a massive star.

While this region of the SMB diagram also has extensive overlap between PNe and H II regions, Abell 48 is plainly not an example of the latter, as its infrared colours (Table 3) reveal. In particular the $[F_{12}/F_8]$ and $[F_{70}/F_{12}]$ ratios strongly indicate a PN rather than a H II region (Anderson et al. 2012).

5.2 Nebular Abundances

In Table 11, we summarise the elemental abundances for the four known PNe with confirmed [WN] or [WN]/[WC] central stars, compared with a selection of ring nebulae around massive stars. Recall that we found Abell 48 to have no significant enrichment of nitrogen, and modest He enrichment, so it does not belong to Peimbert's Type I class (Peimbert 1978; Kingsburgh & Barlow's 1994). We use the nebular argon abundance as a metallicity indicator, as its abundance is predicted to be unaltered by nuclear processes in PN progenitor stars. We conclude that the progenitor of Abell 48 was slightly metal rich with [Ar/H] = +0.12 dex. The metal abundances of PB 8 (Todt et al. 2010a) and IC 4663 (MC12) are similar, and are approximately solar, or slightly more metal rich. We also note that the evolved PNe K 1-27 and LoTr 4, around O(He) stars, also show only modest helium enrichment, but the detailed CNO abundance pattern is difficult to determine for these very high excitation, optically thin PNe (Rauch, Koppen & Werner 1994, 1996).

Also recall that strongly enhanced nitrogen and helium abundances are expected, and seen, in the nebular ejecta around massive LBV stars (Dufour 1989) and WNL stars that remain undiluted by swept-up ISM (Kwitter 1981, 1984; Esteban et al. 1992; Smith et al. 1994; Lamers et al. 2001; Stock et al. 2011). LBV and WR ejecta also show evidence of oxygen depletion (e.g. Dufour 1989), as seen in Table 11, but the oxygen abundance of Abell 48 appears very close to solar. The critical N/O mass ratio is high in LBV and WNL ejecta, ranging up to ∼200 for the ejecta around the peculiar WR star NaSt 1 (Crowther & Smith 1999), while the value for Abell 48 is only 0.12, rather typical of non-Type I PNe (Kingsburgh & Barlow 1994).

5.3 Distance

On the assumption that Abell 48 is a normal planetary, we can calculate a distance using its observed properties. Using the Hα surface brightness – radius (SB-r) relation (Frew & Parker 2006; Frew, Parker & Russeil 2006; Frew 2008), and adopting our angular diameter, reddening, and total Hα flux, we derive a distance of 1.6 ± 0.4 kpc, updated from a preliminary estimate of 2.0 kpc (Bojičić et al. 2012).

We can also determine a kinematic distance if we assume the

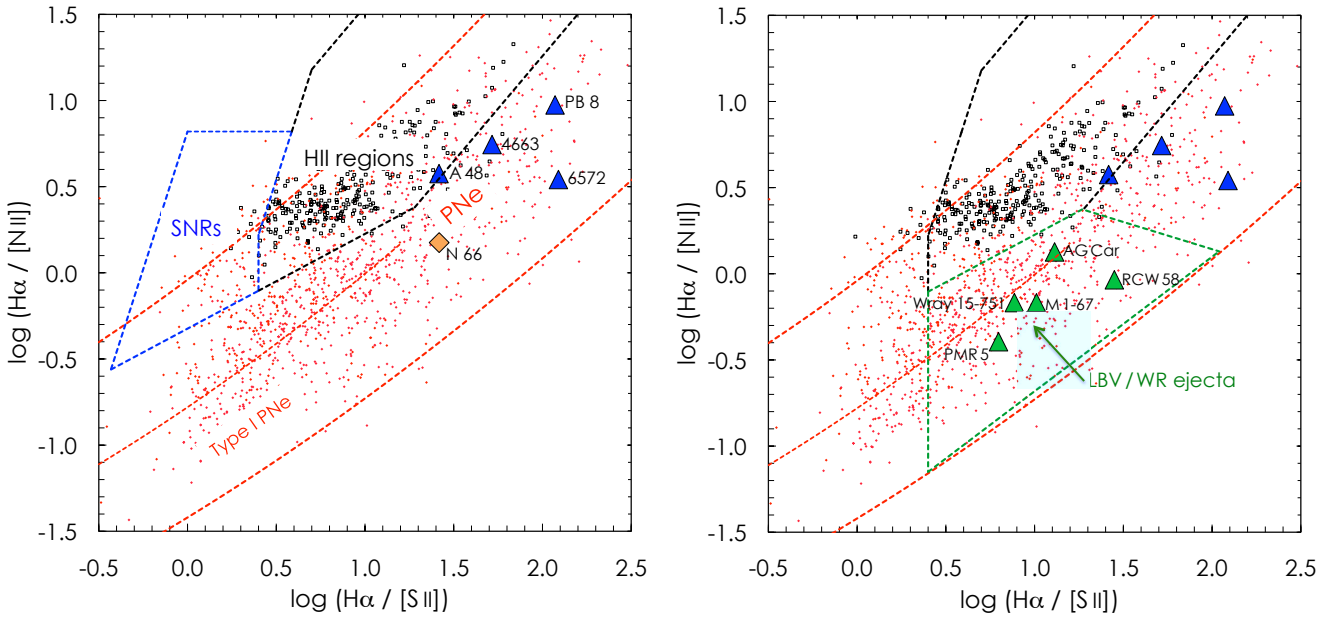

Figure 8. SMB diagnostic plots updated from FP10 (see also Sabin et al. 2012). Individual PNe are shown as small red dots and Galactic H II regions as small black squares. In the left panel the regions populated by HII regions, SNRs and PNe are marked; note the considerable overlap between them. The blue triangles show Abell 48, IC 4663, PB 8, and NGC 6572, which has a candidate [WN/C] CSPN (Todt et al. 2012). These all plot squarely in the PN domain, while the orange diamond is the LMC planetary N 66. In the right panel the domain of LBV/WR ejecta is plotted, and the green triangles plot a selection of ejecta nebulae from the literature.

Table 11. Elemental abundances, normalized to log(H) = 12.0, for the three confirmed Galactic PNe with [WN] or [WN/WC] central stars, and N 66 in the LMC, compared to a sample of ejecta-dominated nebulae around massive stars. The reference sources are given in the footnotes to the table. For comparison, we also list the average abundances for non-Type I and Type I PNe, the abundances of the Orion nebula (a representative H II region) and the solar abundances from Asplund et al. (2009).

Name	SpT	He	N	O	Ne	S	Ar	N/O	[O/H]	[Ar/H]	Reference
Abell 48	[WN4]	11.11	7.78	8.69	8.2:	7.12	6.52	0.12	+0.00	+0.12	This work
IC 4663	[WN3]	11.11	8.26	8.70	8.11	7.02	6.43	0.36	+0.01	+0.03	MC12
PB 8	[WN6/C7]	11.09	8.21	8.76	8.13	7.31	6.64	0.28	+0.07	+0.24	GR09
LMC-N66	[WN4.5]	11.04	7.97	8.37	7.93	6.68	6.11	0.40	−0.32	−0.29	P95,T03,B04
NaSt 1	B[e]/WNL	...	8.87	6.56	7.89	6.94	6.43	200	−2.13	+0.03	CS99
η Car	B[e]/LBV	11.26	9.04	7.29:	7.98	(7.1)	(6.4)	56:	−1.4 :	(0.0)	DG97
AG Car	WN11h	...	8.22	7.52	...	>6.7	...	5.0	−1.17	...	SS97
Hen 3-519	WN11h	...	8.21	7.57	...	...	...	4.4	−1.12	...	S97
Wray 15-751	WN11h	...	8.6:	<8.4	...	...	...	>1.6	<−0.3	...	GL98
M 1-67	WN8h	11.18	8.45	7.98	...	6.96	...	3.0	−0.71	...	EV91
NGC 6888	WN6b(h)	11.27	8.41	8.14	...	7.18	...	1.9	−0.55	...	EV92
NGC 6164-5	O6.5f?p	>11.11	8.13	8.25	7.5:	7.1	>6.3	0.8	−0.44	>−0.1	DP88
Type I PN	...	11.11	8.72	8.65	8.09	6.91	6.42	1.2	−0.04	+0.02	KB94
non-Type I PN	...	11.05	8.14	8.69	8.10	6.91	6.38	0.28	+0.00	−0.02	KB94
Solar	...	10.93	7.83	8.69	7.93	7.12	6.40	0.14	0.00	0.00	AG09
Orion	...	10.99	7.78	8.67	8.05	7.08	6.49	0.13	+0.04	+0.22	D84,EP04
LMC	...	10.99	7.14	8.35	7.61	6.70	6.29	0.06	−0.32	−0.11	RD92

References: AG09 – Asplund et al. (2009); B04 - Bernard-Salas et al. (2004); CS99 – Crowther & Smith (1999); D84 – Dufour (1984); DP88 – Dufour et al. (1988); DG97 – Dufour et al. (1997); EP04 – Esteban et al. (2004); EV91 – Esteban et al. (1991); EV92 – Esteban & Vilchez (1992); GL98 – Garcia-Lario et al. (1998); GR09 – García-Rojas et al. (2009); KB94 – Kingsburgh & Barlow (1994); MC12 – Miszalski et al. (2012b); P95 – Peña et al. (1995); RD92 – Russell & Dopita (1992); S97 – Stroud (1997); SS97 – Smith et al. (1997); T03 – Tsamis et al. (2003).

nebula partakes of circular motion around the Galactic centre. From §3.3.3, we determined $v_{\rm lsr}$ = +49 ± 3 kms^{-1}. The Galactic longitude is favourable for a kinematic distance determination, although with an associated distance ambiguity. Assuming circular rotation, we determine a kinematic distance of either 3.2 ± 1.8 kpc or 12 ± 2.0 kpc where the uncertainty is dominated by the typical velocity dispersion of the respective stellar populations. However, owing to the heavy extinction along this sightline, as discussed in § 3.3.1, we strongly favour a close distance. This result by itself appears to rule out a massive star interpretation (§ 5.4).

5.3.1 Extinction-Distance Relation

As the distance is critical to the interpretation of Abell 48, we revisit this problem here. The stellar 3.6μm and 4.5μm magnitudes along with the available 2MASS photometry implied a large distance of 16.5 kpc on the assumption of Pop I status (Wachter et al. 2010). If this is a Population I star, this distance places it on the far side of the Galactic disk beyond the bulge. The asymptotic reddening in this direction from Schlafly & Finkbeiner (2011, who updated Schlegel et al. 1998) is E(B-V) = 10.0 mag ($A_V \simeq 31$ mag), compared to our own $E(B-V)$ of 1.90 (A_V = 5.9).

Even though the total extinction is not very reliable in this case, there should be at least 15–20 mag of visual extinction if the star is really at or on the far side of the end of the Galactic bar. Hence the discrepancy of such a large distance with a relatively low reddening is difficult to explain if we are dealing with a massive star, a point made by Wachter et al. (2010). The data strongly suggest the star is considerably closer and that it is more likely to be the central star of a PN (see the next section). Our argument is illustrated in Figure 9, which shows the asymptotic reddening as a function of Galactic longitude (Schlafly & Finkbeiner 2011), plotted for two Galactic latitudes, b = 0 (the mid-plane) and b = 0.45 (the latitude of Abell 48). It can be clearly seen that the reddening to Abell 48 is a small fraction of the asymptotic reddening on that sightline, precluding any location for the nebula beyond the Galactic bar.

Figure 10 provides an artist's impression of the Milky Way as viewed from the North Galactic Pole. The position of the Sun and the Galactic centre are indicated by small red circles. The large dotted circle depicts the Solar Circle, and the sightline from the Sun along b = +29° is shown as a white line. The sightline passes close to the intersection of the Galactic Long Bar with the Scutum-Centaurus arm where several major star-forming complexes and young massive clusters occur (Negueruela et al. 2010, 2012, and references therein). The interstellar extinction is heavy in this direction, which militates against the *optical detection* of any emission nebula beyond D = 6 kpc on this sightline.

We adopt the Hα SB-r distance of 1.6 ± 0.4 kpc. The Galactic latitude, b of 0.45°, then gives a $|z|$ height of ∼13 pc, indicating that Abell 48 is almost on the Galactic mid-plane. At this distance, the estimated ionized mass has a sensible value of $M_{\rm ion} \simeq 0.3\sqrt{\epsilon}\ M_\odot$. This is consistent with other PNe, which typically have ionized masses ranging from 5×10^{-3} to 3 $M_\odot$ (FP10). A summary of parameters for the two contrasting interpretations of Abell 48 is presented in Table 12.

5.4 Derived Nebular Properties

In this section we use the surrounding ionized nebula as a diagnostic tool to investigate whether the central star is a massive WN star or a post-AGB star of much lower luminosity. To do this we use the angular diameter, integrated Hα flux and the observed reddening to determine the nebular size and ionized mass, at distances appropriate for the two contrasting interpretations of the central star. In particular, the ionized mass is an important reality check of our distance, and therefore all of the nebular and stellar properties derived from our distance determination.

5.4.1 Nebular Size and Age

Assuming the distance is 1.6 kpc, we arrive at an a nebular mean radius of 0.16 pc, which indicates a middle-aged PN. Using v_{exp} of 40 km s^{-1} from section 3.3.3, we obtain a dynamical age of ∼3900 years with an uncertainty dominated by the distance uncertainty (or 30 per cent). Alternatively, the nebula is ∼2.4 pc across with a dynamical age of 30,000 years (!) if the nucleus is a massive star at a distance of 12 kpc (see above).

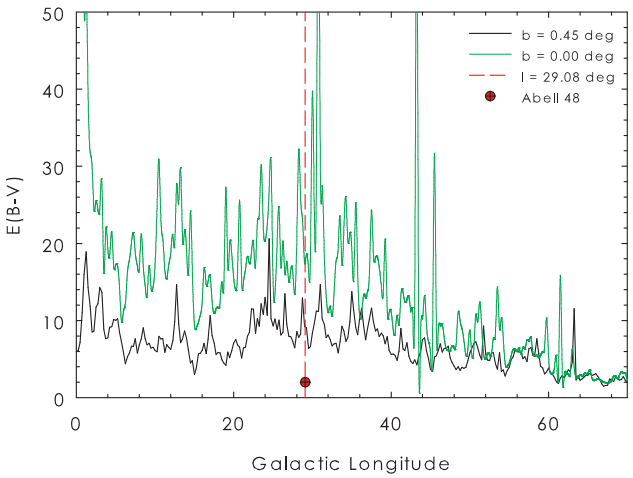

Figure 9. The distribution of reddening with Galactic longitude (Schlafly & Finkbeiner 2011), plotted for two Galactic latitudes, b = 0 (the mid-plane) and b = 0.45 (the latitude of Abell 48). It can be clearly seen that the reddening to Abell 48 is a small fraction of the asymptotic reddening on that sightline, precluding any location for the nebula beyond the Galactic bar.

5.4.2 Ionized mass

We calculated the ionized mass of the nebula following Hua & Kwok (1999), who derived the expression:

$$M_{ion} = 0.032\,(\epsilon/0.6)^{0.5}\theta^{1.5}D^{2.5}F_0(\mathrm{H}\alpha)^{0.5}\,M_\odot \qquad (5)$$

where θ is in arcmin, D is in kpc, and $F_0(\mathrm{H}\alpha) = F(\mathrm{H}\alpha) \times 10^{0.69\times c_{\mathrm{H}\beta}}$ is in units of 10^{-12} erg cm^{-2} s^{-1}, and ϵ is the unknown volume filling factor.

We estimate the mass for two different distance estimates, applicable to a PN central star and a massive WN star. For the massive star interpretation, we simply assume a luminosity typical of a WNE star, $3\times\ 10^5\ L_\odot$, which leads to a distance of 12 kpc, coincidentally the same as the far kinematic distance. However, this distance leads to a nebular mass, $M_{\rm ion} \simeq 50\sqrt{\epsilon}\ M_\odot$, which even allowing for a very low filling factor, can be ruled out, remembering that the total mass, including the dust mass, would be even higher. On the other hand, at a distance of 1.6 kpc, the ionized mass is $0.3\sqrt{\epsilon}\ M_\odot$, a quite typical mass for a planetary nebula (FP10).

5.5 Summary

Based on the overall body of evidence (see FP10) such as its morphology, nebular excitation and abundances, ionized mass, infrared properties, and extinction, Abell 48 is clearly a planetary nebula and not a Population I ring nebula on the far side of the bulge. Table 12 presents an abbreviated comparison of properties assuming Abell 48 is a PN or a Pop I ring nebula respectively.

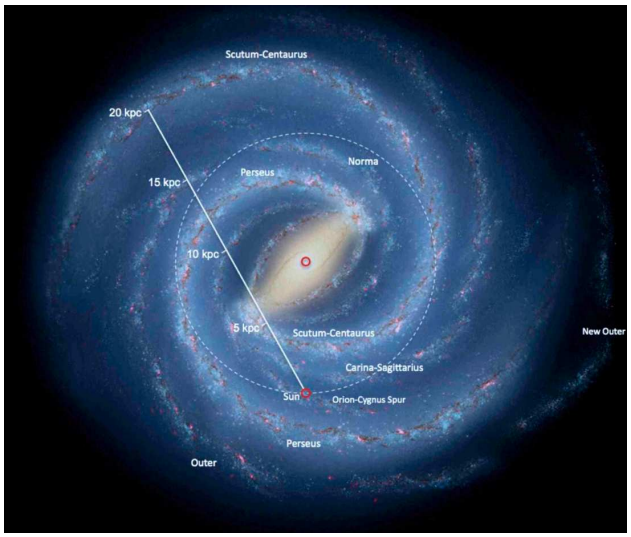

Figure 10. The Milky Way as if viewed from the North Galactic Pole. The position of the Sun and the Galactic centre are indicated by small red circles. The large dotted circle depicts the Solar Circle, and the sightline from the Sun along b = +29° is shown as a white line. The interstellar extinction is heavy in this direction, which militates against the optical detection of any emission nebula beyond D = 6 kpc on this sightline. The base-map was created by Robert Hurt (Spitzer Science Center/Caltech; Credit: NASA/JPL-Caltech/R. Hurt)

Table 12. An abbreviated comparison of quantities, taken from sections 4–6, and a qualitative assessment of the likelihood that Abell 48 a PN or a Population I ring nebula respectively.

Parameter	PN	Ring nebula
D (kpc)	1.6	12.0
R (pc)	0.16	1.2
Dynamical age (yr)	3900	30000
$M_{ion}/M_{\odot}$	$0.3\sqrt{\epsilon}$	$50\sqrt{\epsilon}$
Nebular morphology	✔	✗
Nebular ionized mass	✔	✗
Extinction–distance relation	✔	✗
Diagnostic line ratios	✔	✗
Nebular abundances	✔	✗
Expansion velocity	✔	✔
Nebular MIR colours	✔	✗
MIR/radio flux ratio	✔	✔
Dust temperature	✔	✗
$\|z\|$ distance from Galactic plane	✔	✔

6 ABELL 48 AND THE [WN] CLASS

The [WR] central stars of PNe descend from low- and intermediate-mass progenitors and exhibit a different distribution of subclasses than their massive counterparts. Among the 100+ Galactic central stars, the great majority are classified as [WC] and [WO] stars (Crowther et al. 1998; DePew et al. 2011). The existence of a [WN] class has long been controversial (Hamann et al. 2003; Werner & Herwig 2006; FP10; Todt et al. 2010b; MC12). In the past nitrogen-rich ionizing stars were found in the nebulae M 1-67 (Bertola 1964) and DuRe 1 (Duerbeck & Reipurth 1990). Both were formerly classified as PNe, but are now unambiguously known to be massive WN8 stars surrounded by CNO-processed ejecta (Cohen & Barlow 1975; Crawford & Barlow 1991a, b; Marchenko et al. 2010, and references therein).

Since then, the central stars of LMC N66 (Peña 1995; Peña et al. 2004; Hamann et al. 2003, 2005) and PMR 5 (Morgan, Parker & Cohen 2003) were classified as possible [WN] stars, and a new [WN/WC] class (Todt et al. 2010a,b, 2012) was introduced to accommodate the spectroscopic characteristics of the ionizing star of PB 8. More recently, DePew et al. (2011) identified the CSPN of Abell 48 as either a [WN] or [WN/C] star (cf. Wachter et al. 2010) and the CSPN of IC 4663 was found to be a bona fide [WN3] star (MC12).

The exact nature of of the central star of LMC-N66 is still unclear, but it is likely to be a product of a peculiar binary evolution channel (Hamann et al. 2003). Moreover, we will show in a follow-up paper that PMR 5 is a young, massive WN7b star inside a ring nebula at a distance of 3 – 4 kpc (Frew et al., in preparation; see also Todt et al. 2010b). We briefly summarise these objects in the following sections.

6.1 PMR 5

PHR J1619-4914 is an annular nebula around the WN star PMR 5, that was first discovered as part of the MASH survey (see Parker et al. 2006; Miszalski et al. 2008). Morgan, Parker & Cohen (2003) argued for a status as a PN, and classified the ionizing star as [WN6] based on the detection of the N IV and He II lines in the red. The C IV $\lambda\lambda$5801,5812 doublet appears to be very weak or absent.

However, its PN status was questioned by Werner & Herwig (2006) and Todt et al (2010b). We have now re-classified this star on the basis of a deeper spectrum obtained with WiFeS, and revise the classification to WN7b. We have also found that the surrounding ring nebula is composed of CNO-processed material ejected from a massive star at a distance of about 3.5 kpc. A high-resolution VLT Hα + [N II] image showing a flocculent appearance was published by MC12, and it shows morphological similarities to RCW 58 (Chu 1982; Stock & Barlow 2010) and PCG 11 (Cohen, Parker & Green 2005) which surround WN8h stars. A fuller account on PMR 5 will be published separately (Frew et al., in preparation).

6.2 LMC-N66

LMC-N66 is an unusual, high-excitation, quadrupolar nebula (Peña & Ruiz 1988) in the Large Magellanic Cloud, known also as WS 35 (Westerlund & Smith 1964) and SMP 83 (Sanduleak, MacConnell & Philip 1978). It is ostensibly a PN, as it has a diameter and ionized mass within PN limits. The central star is photometrically and spectroscopically variable, known since McKibben Nail & Shapley (1955) found an amplitude in the V-band of $\sim$1 mag. Dopita et al. (1985) observed a split-profile [O III] λ5007 line, from which they calculated a very high expansion velocity of 85 km s^{-1}. In addition, they found the central star to have a high He Zanstra temperature of 80 kK and an unusually high luminosity of 6×10^4 L$_{\odot}$ (see also Dopita et al. 1993).

A broad He II λ4686 feature was first observed in the spectrum of the CSPN in 1990 (Torres-Peimbert et al. 1993). This feature was not seen earlier in 1985 (Peña & Ruiz 1988), indicating that this represented the onset of a new [WR] outburst phase. The central star of LMC-N66 was first described as a [WN] by Peña (1995), when nitrogen lines at N IV λ3484 and N V λ4606 were noted. In 1994, the UV continuum flux increased four-fold and the optical continuum 25-fold in an eruptive phase (Peña 2002), yet its visual brightness during this outburst only increased by about 0.3 mag, in contrast to the larger variation noted by McKibben Nail & Shapley

(1955). Peña (2002) noted that a high mass-loss rate, $\dot{M} = 2.5\times 10^{-5}$ M$_\odot$ yr^{-1}, was present in 1994.

Such outbursts seems incompatible with our current understanding of CSPNe, and Hamann et al. (2003) have investigated in detail several interpretations for LMC N66. All things considered, they concluded that a binary evolution channel is most likely, either a massive star which has lost its surrounding hydrogen through a common-envelope interaction with a less massive companion, or it represents a (pre)-white dwarf that is rapidly accreting mass from a companion and undergoes quasi-stable nuclear burning. If this is the case, it is probably related to the supersoft X-ray (SSX) sources (Greiner 2000) and their kin, the V Sge stars (Diaz & Steiner 1995; Steiner & Diaz 1998). The latter scenario would suggest that N66 is a potential Type Ia SN progenitor. As also noted by Hamann et al. (2003), SMC N67 is a high-excitation PN exhibiting a similarly high luminosity to N66, but is detectable as an X-ray source (Wang 1991), while N66 is not, perhaps due to absorption of soft X-rays from the PN shell. We note that transient WR winds are also seen in some symbiotic novae (e.g. Thackeray & Webster 1974; Nussbaumer 1996) and is probably due to quasi-stable nuclear burning on the white dwarfs in these binary systems.

6.3 PB 8

The classification of this CSPN has been rather malleable. It was first classified as Of-WR(H) by Méndez (1991), while Parthasarathy, Acker & Stenholm(1998) classified it as a WELS, Acker & Neiner (1993) as a [WC5-6] star, and finally Todt et al. (2010a) named it the prototypical member of the new [WN/WC] class. PB 8 is not a Type I PN, indicating that it has not evolved from massive progenitor. The earlier classification as a [WC5-6] suggests, as with many other H-deficient CSPNe, that differing classifications may result from shallow and/or low-resolution spectra, rather than actual changes in the spectral lines over time. We will return to this object below.

6.4 IC 4663

Recently, MC12 serendipitously discovered a helium-rich [WN3] central star in the bona fide PN IC 4663. At an assumed distance of 3.5 kpc, the V = 16.9 mag central star was estimated to have a temperature of 140 $\pm$ 20kK, and a luminosity of 4000$L_\odot$, quite typical of a central star nearing the knee in its evolutionary track. The properties of the surrounding elliptical PN are also rather typical. The nebula is of high-excitation with a measured expansion velocity, $v_{\rm exp}$ = 30 kms^{-1}, leading to a dynamical age of 4900 years. The star itself is rather weak-lined and is likely close to its evolutionary transformation into a O(He) star (MC12). The surface chemistry is dominated by helium, with a modest amount of nitrogen (only about a quarter that of Abell 48), no sign of hydrogen, and relatively low oxygen abundance.

Figure 11 presents a montage of the three confirmed Galactic PNe with [WN] and [WN/WC] stars, along with the two PNe surrounding O(He) stars, K 1-27 and LoTr 4, included as a morphological comparison. Table 13 compares the fundamental observed and derived properties of Abell 48, IC 4663, and PB 8, and their central stars. All three nebulae are middle-aged, with PB 8 being the smallest object with the highest Hα surface brightness. None of these PNe are particularly luminous, as their absolute λ5007 magnitudes are 2.6 to 3.8 magnitudes below the bright cut-off of the PN luminosity function (e.g. Ciardullo 2010). Furthermore, the fact that none of these nebulae are particularly young leads to the question: what are their progenitors?

Table 13. Properties of Abell 48, IC 4663, and PB 8, and their central stars. The data for IC 4663 and PB 8 come from MC12 and Todt et al. (2010a) respectively, unless otherwise indicated.

Object	Abell 48	IC 4663	PB 8
D (kpc)	1.6	3.5	4.2
Radius (pc)	0.16	0.13	0.07[a]
Kinematic age (yr)	3900	4900	3200[a]
S(Hα)[b] (erg/cm^2/s/sr)	-2.2	-2.2	-1.5
M_{5007}	-0.7	-1.9	-0.7
Spectral type	[WN4]	[WN3]	[WN6/C7]
T_* (kK)	71	140	52
L_* ($L_\odot$)	5500	4000	6000
v_∞ (km s^{-1})	1200	1900	1000
log R_t ($R_\odot$)	0.8	1.13	1.43
R_* ($R_\odot$)	0.49	0.11	0.96
log $\dot{M}$ ($M_\odot$yr^{-1})	$-6.3^{+0.3}_{-0.2}$	$-7.7^{+0.6}_{-0.2}$	$-7.1^{+0.2}_{-0.1}$

Notes: [a]derived from the angular size given by Tylenda et al. (2003); [b]intensity is corrected for reddening.

7 EVOLUTIONARY CONSIDERATIONS

7.1 Elemental Abundances

The surface composition of the central star of Abell 48 (see Table 14) is similar to the products of hydrogen-shell burning, i.e. mainly helium with a moderate amount of nitrogen (see also TK13), though the nitrogen surface abundance in Abell 48 is to our knowledge, the highest known in a post-AGB star. If all the carbon and oxygen in the progenitor was converted to nitrogen via CNO cycling, then the progenitor must have had a substantially supersolar metallicity to explain the high observed nitrogen abundance, but this is marginally inconsistent with the nebular abundances. Otherwise, additional mixing and mass-loss processes have occurred. The existence of [WN/WC] and [WN] central stars implies that there are additional post-AGB evolutionary pathways leading to hydrogen deficiency than previously assumed (De Marco 2002; Werner & Herwig 2006; Werner 2011; FP10; Frew & Parker 2011, 2012), but at present the full diversity of abundances is not explained by stellar evolution theory.

Traditionally, there are three primary post-AGB evolutionary scenarios which are thought to produce H-deficient stars, all of which involve a thermal pulse (Iben et al. 1983; Herwig 2001; Werner & Herwig 2006), but which differ from each other in the point in the stellar evolutionary track when the thermal pulse occurs. These are the AGB Final Thermal Pulse (AFTP), the Late Thermal Pulse (LTP), and the Very Late Thermal Pulse (VLTP) scenarios (see Werner & Herwig 2006, for a review), and the photospheric nitrogen abundance of the star in question is an important diagnostic of the stage during which the final pulse occurs (Werner 2012).

As previously noted, we find a near-canonical Pickering decrement in the central star of Abell 48, which would indicate an absence or low fraction ($\leqslant$10%) of hydrogen, though TK13 estimate an abundance of 10%. In this respect the CSPN of Abell 48 differs both from the [WN/C] ionizing star of PB 8, and the CSPN of IC 4663 (Todt et al. 2010a; MC12). An AFTP is unlikely to produce a star with an abundance pattern as seen in Abell 48, as hydrogen

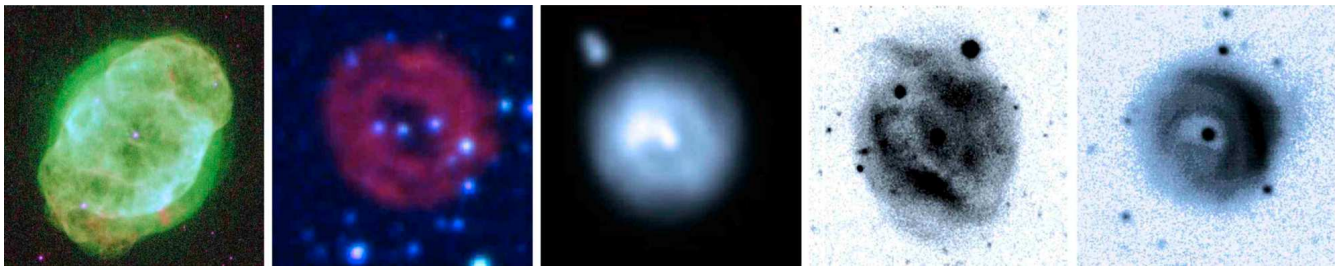

Figure 11. A montage of the bona fide Galactic PNe with [WN] and [WN/WC] CSPNe, plus the PNe K 1-27 and LoTr 4 which surround O(He) stars (not to the same scale). Left to right are IC 4663, Abell 48, PB 8, K 1-27 and LoTr 4. Abell 48 is a Hα/SR/B$_J$ false-colour composite, while the images of IC 4663, PB 8, K 1-27, LoTr 4 are taken from Hajian et al. (2007), Schwarz et al. (1992), Rauch et al. (1998) and Rauch et al. (1996) respectively.

abundances are predicted to exceed 15%, the exact amount depending on the mass of the envelope at the time of the AGB final dredge-up. Moreover, a PG 1159 composition is expected, whereby the C (+O) abundance should greatly exceed the N abundance (Werner & Herwig 2006).

An LTP scenario also seems excluded, as this scenario will reduce the nitrogen abundance to only $\sim$0.1%, and the emission lines attributed to N IV and N V would be expected to be very weak in the optical (Werner et al. 2009). On the other hand a VLTP model requires that the remaining hydrogen will be completely consumed, with surface abundances less than 10^{-7} by mass, however, the observed CNO mass fractions of Abell 48 are not matched by this scenario.

Some additional conclusions about the evolution of the CSPN of Abell 48 can be drawn from nebular abundances. While the low $|z|$-height of Abell 48 is consistent with the scale height of Type I PNe (Frew 2008), the absence of any enrichment of nitrogen shows that hot-bottom burning (e.g. Boothroyd, Sackmann & Ahern 1993) of carbon to nitrogen has not occurred, limiting the progenitor star mass to be less than $\sim$4 $M_{\odot}$.

7.2 Siblings, Progenitors and Progeny

7.2.1 Siblings

Amongst the zoo of post-AGB stars, those that have the most similar surface abundance pattern to Abell 48 and IC 4663 (MC12) are the O(He) stars, of which only four are known, two with surrounding nebulae (Rauch, Dreizler & Wolff 1998; Reindl et al. 2012). However, HS 1522+6615 appears to be carbon rich and nitrogen poor (see Table 14) and it may be unrelated to the other three O(He) stars in an evolutionary sense. Another example might be Abell 52 (Rauch & Kerber 2005), which has the N V$\lambda\lambda$4604,20 lines in emission, and has detectable hydrogen, with He/H = 4 by mass. Similar abundances are also seen in a few, but not all, of the low-gravity, 'luminous' He-sdO stars (e.g. Husfeld et al. 1989; Heber 2009), none of which are convincingly associated with PNe (Méndez et al. 1988).

Table 14 gives a summary of the abundances seen in a range of H-normal and H-deficient post-AGB stars, divided into several tranches on the basis of their atmospheric composition (highlighted in *italics*). The top group are the H-normal stars, and the next two groups are helium-rich, greater than about 80% by mass, but differing in the ratios of N to C+O. The following two groups have substantial residual hydrogen, again separated on their N to C ratios, while the lower three groups include examples with PG1159 abundance patterns (He $\sim$ C $>$ O), hydrogen-rich or 'hybrid' PG1159 compositions (Napiwotzki & Schönberner 1991), and He- *and* H-deficient compositions, respectively.

In fact the luminous He-sdO stars (Jeffery 2008; Napiwotzki 2008; Heber 2009), or alternatively the sdO(He) stars (Rauch et al. 1998) lie in the same region of the Hertzsprung-Russell (HR) diagram[8] as Abell 48. Indeed, a close analogue is the sdO(He) star LSE 263 (Husfeld et al. 1989) but which is not surrounded by any detectable PN. For an earlier discussion on the relationships between the the sdO and O(He) spectral types, see Rauch et al. (1998). Other He-rich stars such as the naked sdO, KS 292 (Rauch et al. 1991), and its PN-shrouded analogue GJJC 1 in M 22 (Harrington & Paltoglou 1993) have rather more hydrogen, and moderate N and C abundances. These examples suggest that there are gradual transitions between the surface compositions of central stars, especially of hydrogen and helium (e.g. Rauch & Kerber 2005), and that the divisions in Table 14 are somewhat arbitrary.

Allowing for the significant observational errors in the gravity determinations, it is feasible that some of the luminous He-sdO stars are just the lower-mass analogues of the [WN] stars. If this is correct, the smaller L/M ratios in the He-sdOs explains the absence of any strong wind features, as they are less proximate to the Eddington Limit, and their lower masses naturally explain the absence of any detectable PNe, owing to the long post-AGB timescales of these 'lazy' remnants (Schönberner 1983; Méndez et al. 1988; Blöcker 1995). Another star with similar abundances, albeit hotter, is the CSPN of LoTr 4 (see Table 14), which is likely to be a descendent of a [WN] star.

7.2.2 Progenitors and Progeny

Werner & Herwig (2006), Werner (2012) and MC12 have commented on the strong compositional and evolutionary links between the O(He) and [WN] stars, but the overall origin of this group of objects is currently being debated. Rauch et al. (2008) have suggested two possible evolutionary scenarios for the formation of the O(He) (and therefore the [WN]) stars. They are either the long-sought successors of the R CrB stars which are strongly H-deficient cool, variable supergiants, that may derive in turn from lower-mass WD mergers (e.g. Clayton et al. 2007), or alternatively, they might be post early-AGB stars or even post-RGB stars (Werner 2012).

[8] The position of the luminous sdO stars in the HR diagram are consistent with post-AGB or post-early AGB evolution (Napiwotzki 2008), while the 'compact' He-rich sdOs are likely to be the product of post-extreme horizontal branch (EHB) evolution (Heber 2009).

Table 14. Properties and elemental surface abundances (expressed as percentage mass fractions) of a selection of post-AGB stars and pre- white dwarfs from the literature, with or without surrounding PNe.

Name	SpT	T_* (kK)	log g (cgs)	$X_{\rm H}$	$X_{\rm He}$	$X_{\rm C}$	$X_{\rm N}$	$X_{\rm O}$	$X_{\rm Ne}$	PN?	Reference
H-rich composition; C + O > N											
K 648	sdO	39	3.9	74	24	0.9	0.001	1.2	...	y	RH02
NGC 6543	Of-[WC]	63	4.7	63	30	1.0	0.2	1.2	...	y	GP08,HB11
NGC 1535	O(H)	85	4.8	74	25	0.2	0.1	0.8	0.2	y	HB04,HB11
Sh 2-216	DAO	95	6.9	95	4	0.1	0.1	0.2	...	y	RZ07
Lo 1	O(H)	120	6.7	69	28	0.2	0.1	2.5	0.2	y	HB04b
He-rich composition; N ≫ C + O											
V652 Her	EHe-B	25	3.7	0.2	99	0.01	0.8	0.04	0.3	n	JH99
LSE 263	sdO(He)	70	4.9	<2	98	0.03	1.6	...	...	n	H89
Abell 48	[WN4]	71	4.9	10:	86:	0.3	4.0:	<0.6	...	y	TK13,FB13
Abell 52	O(He):	110	6.0	20	80	...	pres	...	...	y	RK05
HS2209+8229	O(He)	110	6.0	0.6	99	0.01	0.1	0.02	0.01	n	R12
LoTr 4	O(He)	120	5.5	11	87	<0.7	1.7	<0.09	<0.04	y	R12
K 1-27	O(He)	120	6.0	2	96	0.06	1.7	<0.004	<0.2	y	R12
PG1034+001	DO	120	6.7	<1.2	98	0.02	0.4	0.04	0.13	n†	MR12
PG0038+199	DO	135	7.0	5	93	0.03	1.0	0.1	0.1	n	MR12
IC 4663	[WN3]	140	6.1	<2	>95	<0.1	0.8	0.05	0.2	y	MC12
He-rich composition; C > N											
R CrB	G0 Iab:pe	6.8	0.5	0.001	97	1.4	0.3	1.2	...	(y)	AG00
Sakurai	F5 I	7.3	0.5	0.4	84	5	2	3	6	y	AL99
BD +10°2179	EHe-B	16	2.5	0.01	99	1.7	0.1	0.1	0.1	n	PL11
BD +37°442	sdO(He)	48	4.0	<0.1	97	2.5	0.3	...	...	n	BH95,JH10
LSE 153	sdO(He)	70	4.8	<2	94	5:	0.8	...	...	n	H89
HS1522+6615	O(He)	135	6.0	0.8	99	0.2	0.01	0.1	<0.01	n	WH06,R12
KPD0005+5106	DO	200	6.7	<2.5	98	1.0	0.3	0.4	0.4	n	WW10
He ⩾ H; C ∼ N											
PB 8	[WN6/C7]	52	4.2	40	55	1.3	2.0	1.3	...	y	T10
KS 292	sdO	75	5.0	32	65	2.3	1.3	...	...	n	R91
He ⩾ H; N ≫ C + O											
NGC 2392	O6f	47	4.0	42	57	0.008	0.4	0.01	...	y	MU12,HB11
HD 49798	sdO5.5	47	4.3	19	78	<0.01	2.5	...	...	n	BP97
PG 1159 composition (He ∼ C + O)											
M 2-43	[WC8]	65	4.8	<2	40	50	...	10	...	y	LH98
NGC 40	[WC8]	78	5.0	<2	43	51	...	6	...	y	MD07
V605 Aql	[WC4]	95	...	...	54	40	...	5	...	y	CK06
Abell 78	[WO]-PG1159	115	5.5	...	33	50	2.0	15	...	y	CK06
NGC 6751	[WO4]	135	6.0	...	54	31	1.5	15	...	y	LK93,KH97
PG1159-035	PG1159	140	7.0	<2	33	48	0.1	17	2	n	JR07
K 1-16	PG1159	150	6.1	...	38	56	...	6	...	y	RW95
PG1520+525	PG1159	150	7.5	...	44	39	<0.01	17	...	y	DH98
RXJ2117.1+3412	PG1159	163	6.6	...	39	32	...	22	...	y	CA07
Hybrid PG 1159 composition (He ∼ C > H, O)											
IRAS21282+5050	[WC11]h	28	3.2	10	43	46	<0.5	1.0	...	y	WH06
NGC 7094	PG1159h	100	5.5	17	69	14	0.02	0.2	...	y	ZR09
Abell 43	PG1159h	105	5.6	24	56	19	0.02	0.2	...	y	RF11
HS2324+3944	PG1159h	130	6.2	17	35	42	...	6	...	n	DW96
H- and He-deficient composition (C ∼ O)											
H 1504+65	PG1159pec	200	8.0	...	<1	48	...	48	2	n	WR04

References: AG00 – Asplund et al. (2000); BH95 – Bauer & Husfeld (1995); BP97 – Bisscheroux et al. (1997, and references therein); CA07 – Corsico et al. (2007); CK06 – Clayton et al. (2006); DH98 – Dreizler & Heber (1998); DW96 – Dreizler et al. (1996); FB13 – this work; GOS – Groh, Oliveira & Steiner (2008); H89 – Husfeld et al. (1989); HB04,HB11 – Herald & Bianchi (2004, 2011); JH99 – Jeffery, Hill & Heber (1999); JR07 – Jahn et al. (2007); KH97 – Koesterke & Hamann (1993); LK93 – Leuenhagen et al. (1993); LH96 – Leuenhagen et al. (1996); LH98 – Leuenhagen & Hamann (1998); MC12 – Miszalski et al. (2012b); MD07 – Marcolino et al. (2007); MR12 – Mahsereci et al. (2012); MU12 – Méndez et al. (2012); PL11 – Pandey & Lambert (2011); R91 – Rauch et al. (1991); R12 – Reindl et al. (2012); RF11 – Ringat et al. (2011); RH02 – Rauch et al. (2002); RW95 – Rauch & Werner (1995); RZ07 – Rauch et al. (2007); T10 – Todt et al. (2010a); TK13 – Todt et al. (2013); WH06 – Werner & Herwig (2006); WR04 – Werner et al. (2004); WW10 – Wasserman et al. (2010); ZR09 – Ziegler et al. (2009).

Notes: † PG 1034+001 is the ionizing star of the "planetary nebula" Hewett 1, but this is probably just ionized ambient ISM (Chu et al. 2004; Madsen et al. 2006; Frew 2008).

Indeed, Wassermann et al. (2010) found the very hot, He-burning pre-white dwarf KPD 0005+5106 to have a similar photospheric abundance pattern to the R CrB stars (Clayton 1996; Asplund et al. 2000) and the extreme-helium (EHe) stars (Pandey et al. 2006; Pandey & Lambert 2011). Wassermann et al. (2010) consider both KPD 0005+5106 and the R CrB stars to be WD merger products which form a separate evolutionary post-AGB sequence. It is important to recall that the standard LTP scenario (Herwig 2001; Werner & Herwig 2006) cannot explain the helium-rich abundances seen in these stars.

On theoretical grounds, Saio & Jeffery (2002) concluded that a merger of a CO white dwarf and a less-massive He white dwarf

is a viable model for the formation of the 'majority' R CrB stars, which are compositionally dominated by helium, and have almost negligible hydrogen. More recently, Hema et al. (2012) found that the observed $^{12}C/^{13}C$ isotopic ratios in the majority R CrB stars are also consistent with simple nucleosynthesis predictions for a merger of a CO- with a He-white dwarf (see also Pandey & Lambert 2011; Jeffery, Karakas & Saio 2011). Yet, the observational evidence for R CrB itself is contradictory (Clayton et al. 2011), as the star is surrounded by a substantial nebula (or fossil PN?) suggesting a post-AGB origin. There is also a small group of RCB stars with some residual hydrogen and a peculiar abundance pattern, the so-called 'minority' RCB stars, but their origin is also currently a mystery (Hema et al. 2012; Rao & Lambert 2008).

7.3 Are Binary Channels Needed?

So how do the [WN] stars fit in to this overall framework? The observed atmospheric abundances appear to require the substantial processing of initial carbon and oxygen to nitrogen, followed by removal of the H-rich envelope, possibly via mass transfer in an Algol-type binary system. Recall however, that the nebular abundances for Abell 48 and IC 4663 are very nearly solar (MC12; TK13; and this work), so the observed PN are not simply the stripped atmospheres of these stars. Furthermore, with the exception of a few stars like V652 Her (Jahn et al. 2007), most of the EHe stars (and the R CrB stars) differ from the [WN] stars in having photospheric N $<$ C, suggesting a different evolutionary routes for the two groups. There appears to be a similar dichotomy amongst the O(He) stars, though firm conclusions will only come with a larger sample. Not withstanding these caveats, a binary post-AGB (or even a post-RGB) evolutionary channel with mass exchange (Iben & Tutukov 1985), may be required to produce the [WN] stars, rather than an outright merger (cf. MC12). Guerrero et al. (2013) has suggested an analogous scenario for the formation of the quadrupolar PN, Kn 26 (Jacoby et al. 2010).

Recently, Herald & Bianchi (2011) found the unusual central star of the Eskimo nebula, NGC 2392, to show both a nitrogen enhancement and a deficiency of carbon and oxygen, but with substantial residual hydrogen. This had been earlier noted by Méndez (1991) and Pauldrach, Hoffmann & Méndez (2004). This abundance pattern suggests a second dredge-up may have occurred (e.g. Kingsburgh & Barlow 1994; Marigo et al. 2003), but this is expected only for a narrow range of initial mass, namely between 3–5 $M_{\odot}$. However, other evidence suggests that the Eskimo CSPN is derived from a lower-mass progenitor (Pottasch, Bernard-Salas & Roellig 2008). Interestingly, Méndez et al. (2012) suggest that the abundance pattern of NGC 2392 is the result of truncated evolution due to a close binary interaction, and there is an increasing body of evidence (Pottasch et al. 2008; Danehkar et al. 2012) suggesting that its central star has an accreting compact companion which is detected in hard X-rays (Kastner et al. 2012; Ruiz et al. 2013). So are the [WN] stars also the product of a binary scenario?

Alternatively, there may be other more exotic post-AGB scenarios worth considering, For example, Miller Bertolami et al. (2011) have suggested that diffusion-induced CNO-flashes in a cooling white dwarf (the diffusion-induced nova or DIN scenario) might be applicable to PB 8. While the surface abundance of nitrogen is expected to be enhanced in the DIN scenario, we deem this to be unlikely for Abell 48, as the requirement of a low-mass, low-metallicity white dwarf progenitor does not appear to be met. Furthermore, the mass of the ionized nebula is typical of post-AGB ejected material, and such a significant mass ejection is not expected from a cooling white dwarf with a post-AGB age of 10^6 to 10^7 years (see Miller Bertolami et al. 2011).

Overall, a variety of evolutionary pathways for CSPN evolution is indicated, based on a review of the recent and current literature (e.g. Méndez 1991; Werner 1992; Rauch et al. 1998; Herwig 2001; Blöcker 2001; Werner & Herwig 2006; Todt et al. 2010a; Werner 2012; Quirion, Fontaine & Brassard 2012). Table 15 summarizes these pathways. The first column defines an initial condition for the evolutionary route, the second column gives the route in symbolic form, and the last column gives some candidate examples, primarily drawn from Table 14.

On the basis of the data presented in Table 15, it seems that more theoretical work is required to explain post-AGB stars with an Abell 48-like abundance pattern, with or without residual surface hydrogen. It seems the last two proposed evolutionary pathways are the most viable alternatives, either a previously unknown post-AGB evolutionary route, perhaps a post-early AGB pathway, with mass exchange truncating the evolution, or a binary merger of two white dwarfs.

8 CONCLUSIONS AND FUTURE WORK

On the basis of an extensive set of new and archival observations, we have undertaken a comprehensive analysis of the central star of Abell 48, first classified by Wachter et al. (2010) and De Pew et al. (2011). Based on the presence of very strong N IV lines and moderately strong N V lines at $\lambda\lambda$4604,4620 relative to N III $\lambda\lambda$4634,4640, we now classify it as [WN4] star with little or no hydrogen. We confirm Abell 48 as a bona fide PN after a detailed comparison of the properties of the nebula and its central star. If it was a massive star, the distance would be about 12 kpc, and the ionized mass of the nebula would be nearly $\sim$50 $M_{\odot}$, which is much too high even for a Population I ejecta nebula. Moreover if it were located at or beyond the Galactic Bar, it would suffer much more extinction than observed, and would be optically invisible. We have estimated a new distance of 1.6 kpc, and an ionized mass of $\sim 0.3 M_{\odot}$, a value typical of other PNe. Our results are in substantive agreement with the independent study by TK13.

The recent discovery of bona fide [WN/C] and [WN] central stars show that the diversity of evolutionary pathways leading to PN formation is greater than previously believed (FP10; Frew & Parker 2011; Werner 2012). There are at several more candidate [WN] or [WN/C] stars that we are following up, including PMR 1 (Morgan, Parker & Russeil 2001), PMR 3 (Parker & Morgan 2003), PMR 8 (Mabee 2004), PHR J1757-1649 (DePew et al. 2011); NGC 6572 (Todt et al. 2012) and Kn 15 (Kronberger et al. 2012; Frew et al., in preparation). Another interesting central star is found in the bulge PN, M 1-37 (Kudritzki et al. 1997; Hultzsch et al. 2007) which is a possible [WNL] candidate (see Figure 4 of Kudritzki et al. 1997). As discussed in Frew & Parker (2011, 2012), the current sample of the so-called weak emission-line stars (WELS; Tylenda et al. 1993; Gesicki et al. 2006), a seemingly diverse group, may hold several more [WN] and [WN/C] stars awaiting identification on the basis of better spectra. Indeed, PB 8 was previously identified as a transitional object (Méndez et al. 1989; Parthasarathy et al. 1998) and IC 4663 (Weidmann & Gamen 2011) as a 'WELS' before their discovery as nitrogen-rich [WR] stars.

The relationships of the [WN] and [WN/C] stars to other post-AGB stars are also investigated, and we consider it likely that there are two separate channels producing He-rich stars, as distinct from

Table 15. Potential evolutionary pathways for post-AGB stars.

Initial condition	Pathway	Examples
No final He flash	TP-AGB → O(H) → DAO → DA	NGC 1535, NGC 7293, Sh 2-216
AFTP	TP-AGB → Ofc/[WC] → PG1159h → DA	Abell 43, NGC 7094, Sh 2-68
LTP	post-AGB → AGB → [WC] → [WO] → PG1159 → DO → DB	NGC 40, PG1159-035, PG1520+525
Weak LTP?	post-AGB → AGB → [WN/C]h → DAO → DA	PB 8
VLTP	pre-WD → AGB → [WC] → [WO] → PG1159 → DO → DB	Sakurai's object, FG Sge
Mass transfer / stripping?	eAGB → He-sdO or [WN] → O(He) → DO → DB	Abell 48, N66?
He-WD + CO-WD merger	R CrB → EHe → O(He) → DO → DB	R CrB, KPD 0005+5106?
High-mass progenitor	SAGB → PG1159pec/DO? → hot DQ → DQZ	H1504+65?

the He- and C- dominated PG1159 stars (see Table 14 and Table 15 for examples).

Population modelling should be useful in helping to unravel the origin of the [WN] and related objects. Unfortunately these stars are rare — only three or four Galactic [WN] and [WN/C] stars and four or five O(He) stars are presently known (Rauch et al. 1998, 2009; Reindl et al. 2012; MC12; TK13, and this work). The space density of the O(He) stars is expected to be higher than their [WN] progenitors, in a similar vein to the observed ratio of PG 1159 to [WR] stars in a volume-limited sample of PNe (refer to the data of Frew 2008). This is because the observed space densities are directly related to the time a star spends on the nuclear burning and WD cooling tracks respectively.

Until more [WN] and O(He) stars are identified, and robust estimates of their space density, scale height and birth rate are established, it is will be difficult to fully understand their relationships to other H-deficient stars, and consequently their formation mechanism(s). Time will tell if [WN] central stars are the offspring of binary-induced mass exchange, a WD merger product, or instead represent the progeny of a previously unknown single-star post-AGB evolutionary pathway. It is clear that much more work is still to be done.

ACKNOWLEDGEMENTS

D.J.F. thanks Macquarie University for a MQ Research Fellowship and I.S.B. is the recipient of an Australian Research Council Super Science Fellowship (project ID FS100100019). This research has made use of the SIMBAD database and the VizieR service, operated at CDS, Strasbourg, France.

REFERENCES

Abell G.O., 1955, PASP, 67, 258
Abell G.O., 1966, ApJ, 144, 259
Acker A., Ochsenbein F., Stenholm B., Tylenda R., Marcout J., Schohn C., 1992, Strasbourg-ESO Catalogue of Galactic Planetary Nebulae (Garching: ESO)
Acker A., Neiner C., 2003, A&A, 403, 659
Ali A., Sabin L., Snaid S., Basurah H.M., 2012, A&A, 541, A98
Allamandola L. J., Tielens A.G.G.M., Barker J.R., 1989, ApJS, 71, 733
Anderson L.D., Zavagno A., Barlow M.J., Garca-Lario P., Noriega-Crespo A., 2012, A&A, 537, A1
Asplund M., Gustafsson B., Lambert D.L., Rao N.K., 2000, A&A, 353, 287
Asplund M., Grevesse N., Sauval A.J., Scott P., 2009, ARA&A, 47, 481
Bauer F., Husfeld D., 1995, A&A, 300, 481
Benjamin R.A. et al., 2003, PASP, 115, 953
Bernard-Salas J., Houck J.R., Morris P.W., Sloan G.C., Pottasch S.R., Barry D.J., 2004, ApJS, 154, 271
Bertola F., 1964, PASP, 76, 241
Bisscheroux B.C., Pols O.R., Kahabka P., Belloni T., van den Heuvel E.P.J., 1997, A&A, 317, 815
Blöcker T., 1995, A&A, 299, 755
Blöcker T., 2001, Ap&SS, 275, 1
Bojičić I.S., Parker Q.A., Filipović M.D., Frew D.J., 2011a, MNRAS, 412, 223
Bojičić I.S., Parker Q.A., Frew D.J., Vaughan A.E., Filipović M.D., Gunawardhana M.L.P., 2011b, AN, 332, 697
Bojičić I.S., Frew D.J., Parker Q.A., Stupar M., Wachter S., DePew K., 2012, ASP Conf. Proc., in press (arXiv:1212.5382)
Boothroyd A.I., Sackmann I.-J., Ahern S.C., 1993, ApJ, 416, 762
Borkowski K.J., Sarazin C.L., Soker N., 1990, ApJ, 360, 173
Chu Y.-H., 1982, ApJ, 254, 578
Chu Y.-H., 2003, IAUS, 212, 585
Chu Y.-H., Gruendl R.A., Williams R.M., Gull T.R., Werner K., 2004, AJ, 128, 2357
Ciardullo R., 2010, PASA, 27, 149
Clayton G.C., 1996, PASP, 108, 225
Clayton G.C., Kerber F., Pirzkal N., De Marco O., Crowther P.A., Fedrow J.M., 2006, ApJ, 646, L69
Clayton G.C., Geballe T.R., Herwig F., Fryer C., Asplund M., 2007, ApJ, 662, 1220
Clayton G.C. et al., 2011a, AJ, 142, 54
Clayton G.C. et al., 2011b, ApJ, 743, 44
Cohen M., Barlow M.J., 1975, ApL, 16, 165
Cohen M., Parker Q.A., Green A.J., 2005, MNRAS, 360, 1439
Cohen M. et al., 2007, ApJ 669, 343
Cohen M., Parker Q.A., Green A.J., Miszalski B., Frew D.J., Murphy T., 2011, MNRAS, 413, 514
Condon J.J., Cotton W.D., Greisen E.W., Yin Q.F., Perley R.A., Taylor G.B., Broderick J.J., 1998, AJ, 115, 1693
Condon J.J., Kaplan D.L., 1998, ApJS, 117, 361
Conti P.S., Massey P., Vreux J.-M., 1990, ApJ, 354, 359
Córsico A.H., Althaus L.G., Miller Bertolami M.M., Werner K., 2007, A&A, 461, 1095
Crawford I.A., Barlow M.J., 1991a, A&A, 249, 518
Crawford I.A., Barlow M.J., 1991b, A&A, 251, L39
Crowther P.A., 2007, ARA&A, 45, 177
Crowther P.A., 2008, ASPC, 391, 83
Crowther P.A., Smith L.J., 1999, MNRAS, 308, 82
Crowther P.A., Morris P.W., Smith J.D., 2006, ApJ, 636, 1033
Crowther P.A., De Marco O., Barlow M.J., 1998, MNRAS, 296, 367
Danehkar A., Frew D.J., Parker Q.A., De Marco O., 2012, IAUS, 282, 470
De Marco O., 2002, Ap&SS, 279, 157
De Marco O., Storey P.J., Barlow M.J., 1998, MNRAS, 297, 999
De Marco O., Clayton G.C., Herwig F., Pollacco D.L., Clark J.S., Kilkenny D., 2002, AJ, 123, 3387
De Marco O., Hillwig T.C., Smith A.J., 2008, AJ, 136, 323
De Marco O., Passy J.-C., Frew D.J., Moe M.M., Jacoby G.H., 2013, MN-

RAS, 428, 2118
DePew K., 2011, PhD thesis, Macquarie University
DePew K., Parker Q.A., Miszalski B., De Marco O., Frew D.J., Acker A., Kovacevic A.V., Sharp R.G., 2011, MNRAS, 414, 2812
Dopita M.A., Meatheringham S.J., 1990, ApJ, 357, 140
Dopita M.A., Ford H.C., Webster B.L., 1985, ApJ, 297, 593
Dopita M.A., Ford H.C., Bohlin R., Evans I.N., Meatheringham S.J., 1993, ApJ, 418, 804
Dopita M., Hart J., McGregor P., Oates P., Bloxham G., Jones D., 2007, Ap&SS, 310, 255
Dopita M.A. et al., 2010, Ap&SS, 327, 245
Douchin D. et al., 2012, IAUS, 283, 346
Duerbeck H.W., Reipurth B., 1990, A&A, 231, L11
Dufour R.J., 1984, IAUS, 108, 353
Dufour R.J., 1989, RMxAA, 18, 87
Dufour R.J., Parker R.A.R., Henize K.G., 1988, ApJ, 327, 859
Dufour R.J., Glover T.W., Hester J.J., Currie D.G., van Orsow D., Walter D.K., 1997, ASPC, 120, 255
Dreizler S., Heber U., 1998, A&A, 334, 618
Dreizler S., Werner K., Heber U., Engels D., 1996, A&A, 309, 820
Egan M.P. et al., 2003, Air Force Research Laboratory Technical Report AFRL-VS-TR-2003-1589
Epchtein N. et al., 1994, Ap&SS, 217, 3
Ercolano B., Barlow M.J., Storey P.J., Liu X.-W., 2003, MNRAS, 340, 1136
Ercolano B., Barlow M.J., Storey P.J., 2005, MNRAS, 362, 1038
Esteban C., Vilchez J.M., 1992, ApJ, 390, 536
Esteban C., Vilchez J.M., Manchado A., Smith L.J., 1991, A&A, 244, 205
Esteban C., Peimbert M., García-Rojas J., Ruiz M.T., Peimbert A., Rodríguez M., 2004, MNRAS, 355, 229
Fernández-Martn A. Martn-Gordón D., Vlchez J.M., Pérez Montero E., Riera A., Sánchez S.F., 2012, A&A, 541, A119
Frew D.J., 2008, PhD Thesis, Macquarie University
Frew D.J., Parker Q.A., 2006, IAUS, 234, 49
Frew D.J., Parker Q.A., 2010, PASA, 27, 129 (FP10)
Frew D.J., Parker Q.A., 2011, Proc. APN V Conference, 33
Frew D.J., Parker Q.A., 2012, IAUS, 283, 192
Frew D.J., Parker Q.A., Russeil D., 2006, MNRAS, 372, 1081
Frew D.J. et al., 2011, PASA, 28, 83
Frew D.J., Bojičić I.S., Parker Q.A., 2012, IAUS, 283, 362
Frew D.J., Bojičić I.S., Parker Q.A., 2013a, MNRAS, in press (arXiv:1211.2505)
Frew D.J., Bojičić I.S., Parker Q.A., Pierce M.J., Gunawardhana M.L.P., Reid W.A., 2013b, MNRAS, submitted
Friedman S.D. et al., 2011, ApJ, 727, 33
Garcia-Lario P., Riera A., Manchado, A., 1998, A&A, 334, 1007
García-Rojas J., Peña M., Peimbert A., 2009, A&A, 496, 139
Gaustad J.E., McCullough P.R., Rosing W., Van Buren D., 2001, PASP, 113, 1326
Gesicki K. et al., 2006, A&A, 451, 925
Gooch R., 1996, ASPC, 101, 80
Gräfener G., Koesterke L., Hamann W.-R., 2002, A&A, 387, 244
Greiner J., 2000, NewA, 5, 137
Groh J.H., Oliveira A.S., Steiner J.E., 2008, A&A, 485, 245
Gruendl R.A., Chu Y.-H. Dunne B.C., Points S.D., 2000, AJ,120, 2670
Guerrero M.A., Miranda L.F., Ramos-Larios G., Vázquez R., 2013, A&A, 551, A53
Gvaramadze V.V., Kniazev A.Y., Fabrika S., 2010, MNRAS, 405, 1047
Hajduk M., Zijlstra A.A., Gesicki K., 2010, MNRAS, 406, 626
Hajian A. et al., 2007, ApJS, 169, 289
Hamann W.-R., Koesterke L., 1998, A&A, 333, 251
Hamann W.-R., Gräfener G., 2003, A&A, 410, 993
Hamann W.-R., Gräfener G., 2004, A&A, 427, 697,
Hamann W.-R., Koesterke L., Wessolowski U., 1995, A&AS, 113, 459
Hamann W.-R., Peña M., Gräfener G., Ruiz M.T., 2003, A&A, 409, 969
Hamann W.-R., Peña M., Gräfener G., 2005, ASPC, 334, 345
Hamann W.-R., Gräfener G., Liermann A., 2006, A&A, 457, 101
Hambly N.C. et al., 2001, MNRAS, 326, 1279
Harrington J.P., Paltoglou G., 1993, ApJ, 411, L103
Heber U., 2009, ARA&A, 47, 211
Helfand D.J., Becker R.H., White R.L., Fallon A., Tuttle S., 2006, AJ, 131, 2525
Herald J.E., Bianchi L., 2011, MNRAS, 417, 2440
Herwig F., 2001, Ap&SS, 275, 15
Howarth I.D., 1983, MNRAS, 203, 301
Hua C.T., Kwok S., 1999, A&AS, 138, 275
Hultzsch P.J.N., Puls J., Méndez R.H., Pauldrach A.W.A., Kudritzki R.-P., Hoffmann T.L., McCarthy J.K., 2007, A&A, 467, 1253
Hummer D.G., Storey P.J., 1987, MNRAS, 224, 801
Husfeld D., Butler K., Heber U., Drilling J.S., 1989, A&A, 222, 150
Iben I. Jr., 1984, ApJ, 277, 333
Iben I. Jr., 1990, ApJ, 353, 215
Iben I. Jr., Renzini A., 1983, ARA&A, 21, 271
Iben I. Jr., Tutukov A.V., 1985, ApJS, 58, 661
Iben I. Jr., Kaler J.B., Truran J.W., Renzini A., 1983, ApJ, 264, 605
Indebetouw R. et al., 2005, ApJ, 619, 931
IPAC, 1986, IRAS Catalog of Point Sources, Version 2.0, VizieR online catalogue, II/125
Ishihara D. et al., 2010, A&A, 514, A1
Jahn D., Rauch T., Reiff E., Werner K., Kruk J.W., Herwig F., 2007, A&A, 462, 281
Jeffery C.S., 2008, ASPC, 391, 3
Jeffery C.S., Hill P.W., Heber U., 1999, A&A, 346, 491
Jeffery C.S., Karakas A.I., Saio H., 2011, MNRAS, 414, 3599
Jorissen A., Frankowski A., 2008, AIPC, 1057, 1
Kastner J.H. et al., 2012, AJ, 144, 58
Kimeswenger S. et al., 1998, A&A, 332, 300
Kingsburgh R.L., Barlow M.J., 1994, MNRAS, 271, 257
Koesterke L., Hamann W.-R., 1997, A&A, 320, 91
Kohoutek L., 2001, A&A, 378, 843
Kronberger M. et al., 2012, IAUS, 283, 414
Kudritzki R.P., Méndez R.H., Puls J., McCarthy J.K., 1997, IAUS, 180, 64
Kwitter K.B., 1981, ApJ, 245, 154
Kwitter K.B., 1984, ApJ, 287, 840
Kwok S., Zhang Y., Koning N., Huang H.-H., Churchwell E., 2008, ApJS, 174, 426
Lamers H.J.G.L.M., Nota A., Panagia N., Smith L.J., Langer N., 2001, ApJ, 551, 764
Landolt A.U., 2009, AJ, 137, 4186
Lanz T., Hubeny I., Heap S.R., 1997, ApJ, 485, 843
Lawrence A. et al., 2007, MNRAS, 379, 1599
Leuenhagen U., Hamann W.-R., 1998, A&A, 330, 265
Leuenhagen U., Koesterke L., Hamann W.-R., 1993, AcA, 43, 329
López J.A., Richer M.G., Garca-Díaz, M.T., Clark D.M., Meaburn J., Riesgo H., Steffen W., Lloyd M., 2012, RMxAA, 48, 3
Mabee A., 2004, BSc (Honours) Thesis, Macquarie University
Madsen G.J., Frew D.J., Parker Q.A., Reynolds R.J., Haffner L.M., 2006, IAUS, 234, 455
Mahsereci M., Ringat E., Rauch T., Werner K., Kruk J.W., 2012, IAUS, 283, 426
Marchenko S.V., Moffat A.F.J., Crowther P.A., 2010, ApJ, 724, L90
Marcolino W.L.F., Hillier D.J., de Araujo F.X., Pereira C.B., 2007, ApJ, 654, 1068
Marigo P., Bernard-Salas J., Pottasch S.R., Tielens A.G.G.M. Wesselius P.R., 2003, A&A, 409, 619
McKibben Nail V., Shapley H., 1955, PNAS, 41, 685
Medina S., Peña M., Morisset C., Stasińska G., 2006, RMxAA, 42, 53
Méndez R.H., 1989, IAUS, 131, 261
Méndez R.H., 1991, IAUS, 145, 375
Méndez R.H., Gathier R., Simon K.P., Kwitter K.B., 1988, A&A, 198, 287
Méndez R.H., Urbaneja, M.A., Kudritzki, R.P., Prinja, R.K., 2012, IAUS, 283, 436
Miller Bertolami M.M., Althaus L.G., 2006, A&A, 454, 845
Miller Bertolami M.M., Althaus L.G., Olano C., Jiménez N., 2011, MNRAS, 415, 1396
Miszalski B., Parker Q.A., Acker A., Birkby J.L., Frew D.J., Kovacevic A., 2008, MNRAS, 384, 525

Miszalski B., Acker A., Parker Q.A., Moffat A.F.J., 2009, A&A, 496, 813
Miszalski B., Boffin H.M.J., Frew D.J., Acker A., Köppen J., Moffat A.F.J., Parker Q.A., 2012a, MNRAS, 419, 39
Miszalski B., Crowther P.A., De Marco O., Köppen J., Moffat A.F.J., Acker A., Hillwig T.C., 2012b, MNRAS, 423, 934 (MC12)
Mizuno D.R., et al., 2010, AJ, 139, 1542
Monet D.G. et al., 2003, AJ, 125, 984
Morgan D.H., Parker Q.A., Cohen M., 2003, MNRAS 346, 719
Napiwotzki R., 2008, ASPC, 391, 257
Napiwotzki R., Schönberner D., 1991, A&A, 249, L16
Negueruela I., González-Fernández C., Marco A., Clark J.S., Martínez-Núñez S., 2010, A&A, 513, A74
Negueruela I., Marco A., González-Fernández C., Jiménez-Esteban F., Clark J.S., Garcia M., Solano E., 2012, A&A, 547, A15
Nieva M.-F., Przybilla N., 2012, A&A, 539, A143
Nussbaumer H., 1996, Ap&SS, 238, 125
O'Dell C.R., Ferland G.J., Henney W.J., Peimbert M., 2013, AJ, 145, 92
Oliveira A.S., Steiner J.E., Cieslinski D., 2003, MNRAS, 346, 963
Paladini R., Burigana C., Davies R.D., Maino D., Bersanelli M., Cappellini B., Platania P., Smoot G., 2003, A&A, 397, 213
Pandey G., Lambert D.L., 2011, ApJ, 727, 122
Pandey G., Lambert D.L., Jeffery C.S., Rao N.K., 2006, ApJ, 638, 454
Parker Q.A., Morgan D.H., 2003, MNRAS, 341, 961
Parker Q.A. et al., 2005, MNRAS, 362, 689
Parker Q.A. et al., 2006, MNRAS, 373, 79
Parker Q.A. et al., 2012, MNRAS, 427, 3016
Parthasarathy M., Acker A., Stenholm B., 1998, A&A, 329, L9
Pauldrach A.W.A., Hoffmann T.L., Méndez R.H., 2004, A&A, 419, 1111
Peimbert M., 1978, IAUS, 76, 215
Peimbert M., Torres-Peimbert S., 1983, IAUS, 103, 233
Peña M., 1995, RMxAC, 3, 215
Peña M., 2002, RMxAC, 12, 148
Peña M., Ruiz M.T., 1988, RMxAA, 16, 55
Peña M., Peimbert M., Torres-Peimbert S., Ruiz M.T., Maza J., 1995, ApJ, 441, 343
Peña M., Hamann W.-R., Koesterke L., Maza J., Méndez R.H., Peimbert M., Ruiz M.T., Torres-Peimbert S., 1997, ApJ, 491, 233
Peña M. et al., 1998, RMxAC, 7, 215
Peña M., Medina S., Stasińska G., 2003, RMxAC, 15, 38
Peña M., Peimbert A., Hamann W.-R., Ruiz M.T., Peimbert M., 2004, ASPC, 313, 131
Peña M., Ruiz M.T., Rojo P., Torres-Peimbert S., Hamann, W.-R., 2008, ApJ, 680, L109
Phillips J.P., Marquez-Lugo R.A., 2011, MNRAS, 410, 2257
Pierce M.J., Frew D.J., Parker Q.A., Köppen J., 2004, PASA, 21, 334
Pottasch S.R., Bernard-Salas J., Roellig T.L., 2008, A&A, 481, 393
Quirion P.-O., Fontaine G., Brassard P., 2012, ApJ, 755, 128
Rauch T., Kerber F., 2005, ASPC, 334, 329
Rauch T., Werner K., 1995, Lecture Notes in Physics, 443, 186
Rauch T., Dreizler S., Wolff B., 1998, A&A, 338, 651
Rauch T., Köppen J., Werner K., 1996, A&A, 310, 613
Rauch T., Heber U., Werner K., 2002, A&A, 381, 1007
Rauch T., Reiff E., Werner K., Herwig F., Koesterke L., Kruk J.W., 2006, ASPC, 348, 194
Rauch T., Reiff E., Werner K., Kruk J.W., 2008, ASPC, 391, 135
Rauch T., Werner K., Kruk J.W., 2009, AIPC, 1135, 168
Reid W.A., Parker Q.A., 2010, PASA, 27, 187
Ringat E., Friederich F., Rauch T., Werner K., Kruk J.W., 2011, Proc. APN V Conference, 165
Rodríguez-Gil P. et al., 2010, MNRAS, 407, L21
Roeser S., Demleitner M., Schilbach E., 2010, AJ, 139, 2440
Ruiz N., Chu Y.-H., Gruendl R.A., Guerrero M.A., Jacob R., Schönberner D., Steffen M., 2013, ApJ, in press (arXiv:1302.3886)
Russell S.C., Dopita M.A., 1992, ApJ, 384, 508
Sabbadin F., Minello S., Bianchini A., 1977, A&A, 60, 147
Sabin L. et al., 2013, MNRAS, tmp833 (arXiv:1301.6416)
Saio H., Jeffery C.S., 2002, MNRAS, 333, 121
Sanduleak N., MacConnell D.J., Philip A.G.D., 1978, PASP, 90, 621
Schlafly E.F., Finkbeiner D.P., 2011, ApJ, 737, 103
Schlegel D.J., Finkbeiner D.P., Davis M., 1998, ApJ, 500, 525
Schmutz W., Hamann W.-R., Wessolowski U., 1989, A&A, 210, 236
Schönberner D., 1983, ApJ, 272, 708
Schönberner D., Jacob R., Steffen M., Perinotto M., Corradi R.L.M., Acker A., 2005, A&A, 431, 963
Schwarz H.E., Corradi R.L.M., Melnick J., 1992, A&AS, 96, 23
Skrutskie M.F. et al., 2006, AJ, 131, 1163
Smith L.F., Meynet G., Mermilliod J.-C., 1994, A&A, 287, 835
Smith L.F., Shara M.M., Moffat A.F.J. 1996, MNRAS, 281, 163
Smith L.J. Stroud M.P., Esteban C., Vilchez J.M., 1997, MNRAS, 290, 265
Soker N., 1997, ApJS, 112, 487
Soker N., Borkowski K.J., Sarazin C.L., 1991, AJ, 102, 1381
Spitzer L., 1978, Physical processes in the interstellar medium. New York: Wiley-Interscience
Stasińska G., Szczerba R., Schmidt M., Siódmiak N., 2006, A&A, 450, 701
Steiner J.E., Diaz M.P., 1998, PASP, 110, 276
Steiner J.E., Oliveira A.S., 2005, A&A, 444, 895
Stock D.J., Barlow M.J., 2010, MNRAS, 409, 1429
Stock D.J., Barlow M.J., Wesson R., 2011, MNRAS, 418, 2532
Stroud M.P., 1997, ASPC, 120, 349
Thackeray A.D., Webster B.L., 1974, MNRAS, 168, 101
Todt H., Gräfener G., Hamann W.-R., 2006, IAUS, 234, 127
Todt H., Peña M., Hamann W.-R., Gräfener G., 2010a, A&A, 515, 83
Todt H., Peña M., Hamann W.-R., Gräfener G., 2010b, AIPC, 1273, 219
Todt H., Peña M., Zühlke J., Oskinova L., Hamann W.-R., Gräfener G., 2012, IAUS, 283, 510
Todt H. et al., 2013, MNRAS, accepted (arXiv:1301.1944) (TK13)
Torres-Peimbert S., Peimbert M., Ruiz M.T., Peña M., 1993, IAUS, 155, 584
Tsamis Y.G., Barlow M.J., Liu X.-W., Danziger I.J., Storey P.J., 2003, MNRAS, 345, 186
Tylenda R., Acker A., Stenholm B. 1993, A&AS, 102, 595
Tylenda R., Siódmiak N., Górny S.K., Corradi R.L.M., Schwarz H.E., 2003, A&A, 405, 627
van der Hucht K.A., Jurriens T.A., Wesselius P.R., Olnon F.M., The P.S., Williams P.M., 1985, A&A, 145, 13
Vreux J.M., Dennefeld M., Andrillat Y., 1983, A&AS, 54, 437
Wachter S., Mauerhan J.C., Van Dyk S.D., Hoard D.W., Kafka S., Morris P.W., 2010, AJ, 139, 2330
Wang Q., 1991, MNRAS, 252, P47
Wareing C.J., 2010, PASA, 27, 220
Wareing C.J., O'Brien T.J., Zijlstra A.A. Kwitter K.B., Irwin J., Wright N., Greimel R., Drew, J.E., 2006, MNRAS, 366, 387
Wassermann D., Werner K., Rauch T., Kruk J.W., 2010, A&A, 524, A9
Weidmann W.A., Gamen R., 2011, A&A, 531, A172
Werner K., 1992, Lecture Notes in Physics, 401, 273
Werner K., 2012, IAUS, 283, 196
Werner K., Herwig F., 2006, PASP, 118, 183
Werner K., Rauch T., Barstow M.A., Kruk J.W., 2004, A&A, 421, 1169
Werner K., Jahn D., Rauch T., Reiff E., Herwig F., Kruk J.W., 2006, MmSAI, 77, 996
Werner K., Rauch T., Reiff E., Kruk J.W., 2009, Ap&SS, 320, 159
Wesson R., Stock, D.J., Scicluna P., 2012, MNRAS, 422, 3516
Woudt P.A. et al., 2009, ApJ, 706, 738
Zacharias N., Monet D.G., Levine S.E., Urban S.E., Gaume R., Wycoff G.L., 2004, AAS, 205, 48.15
Zhang Y., Liu X.-W., Liu Y., Rubin R.H., 2005, MNRAS, 358, 457
Ziegler M., Rauch T., Werner K., Koesterke L., Kruk J.W., 2009, Communications in Asteroseismology, 159, 107